

Short-range correlation physics at low renormalization group (RG) resolution

Anthony Tropiano¹, Scott Bogner², Dick Furnstahl¹

¹Ohio State University, ²Michigan State University

Los Alamos seminar

December 15, 2021

ajt, S.K. Bogner, and R.J. Furnstahl, arXiv:2105.13936

*Phys. Rev. C **104**, 034311 (2021)*

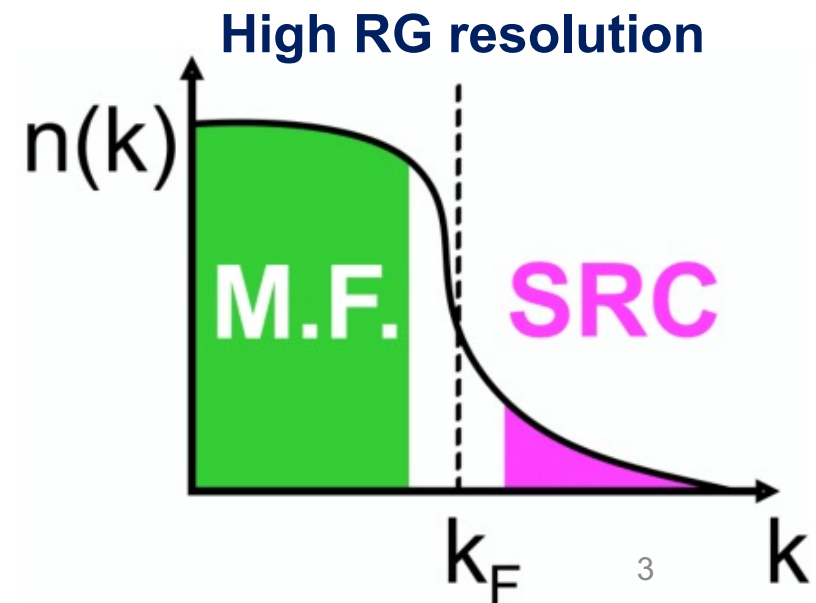


Short-range correlations

- Recent experiments have been able to isolate processes where short-range correlation (SRC) physics is dominant and well accounted for by SRC phenomenology
- How are short-range correlations defined?
 - Depends on the resolution scale!
 - Renormalization group (RG) resolution scale is set by Λ in the Hamiltonian $H(\Lambda)$
 - $\Lambda \sim$ max momenta in low-energy wave functions

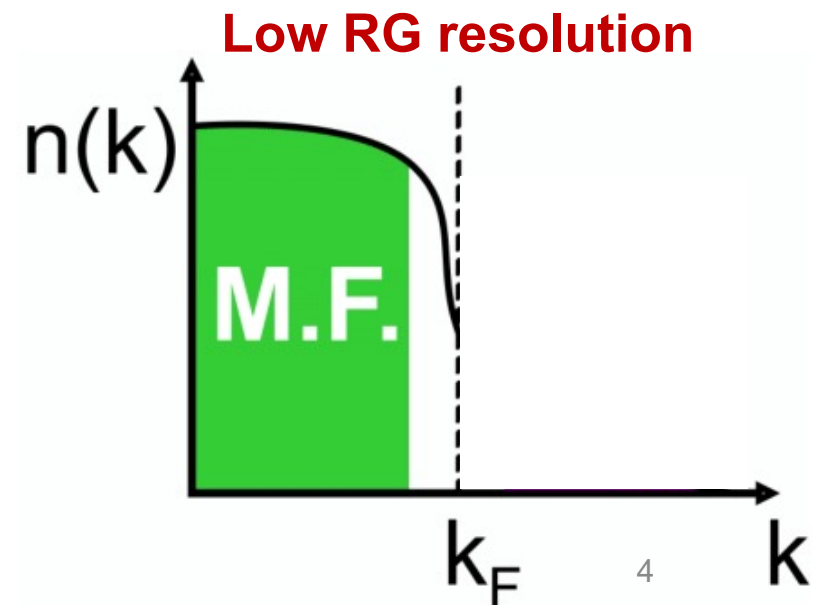
High and low RG resolution

- SRC physics at high RG resolution
 - SRC pairs are components in the nuclear wave function with relative momenta well above the Fermi momentum k_F and CM momentum $< k_F$



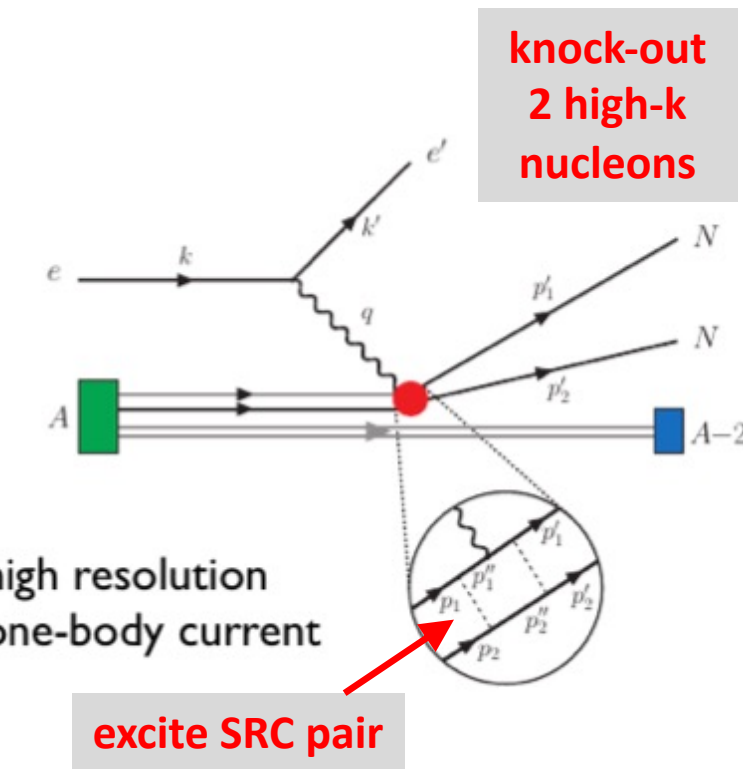
High and low RG resolution

- SRC physics at high RG resolution
 - SRC pairs are components in the nuclear wave function with relative momenta well above the Fermi momentum k_F and CM momentum $< k_F$
- SRC physics at low RG resolution
 - The SRC *physics* is shifted into the reaction operators from the nuclear wave function (which becomes soft)



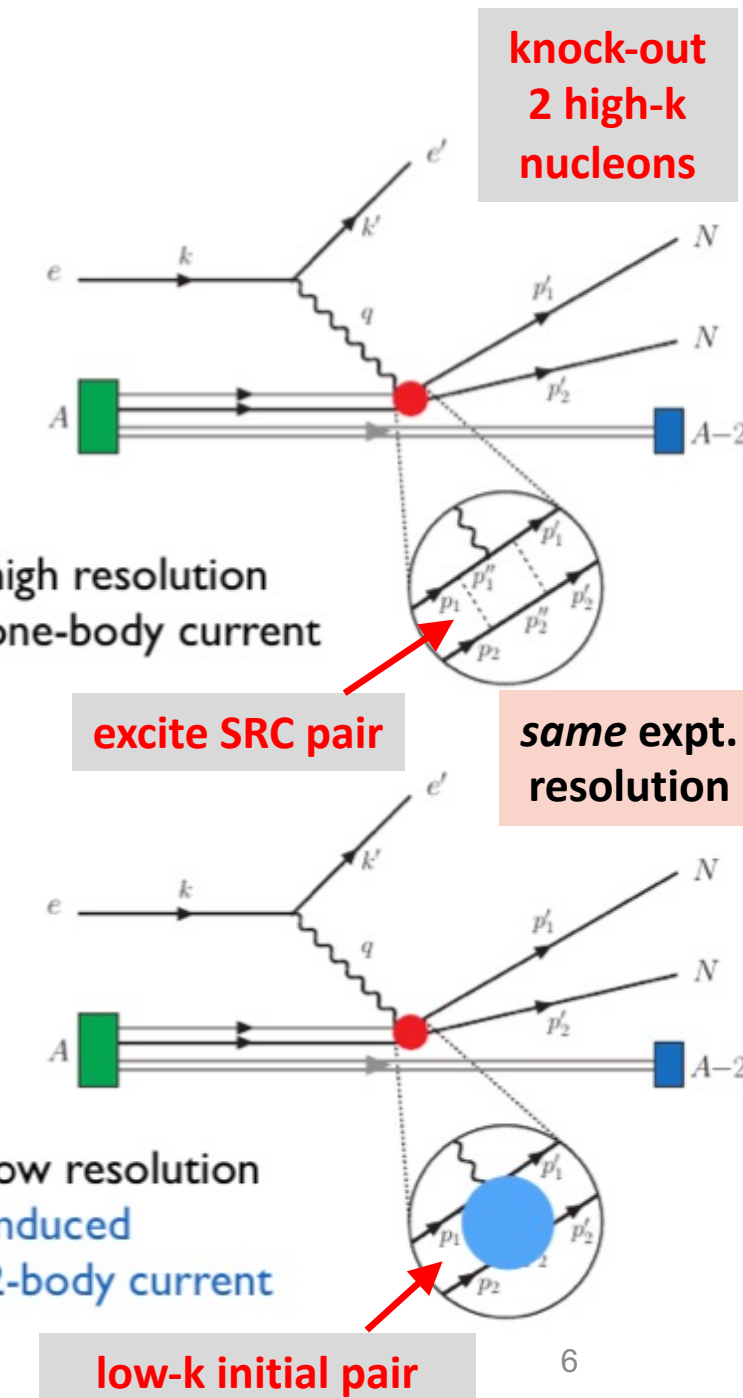
High and low RG resolution

- High RG resolution: One-body current operators with correlated wave functions



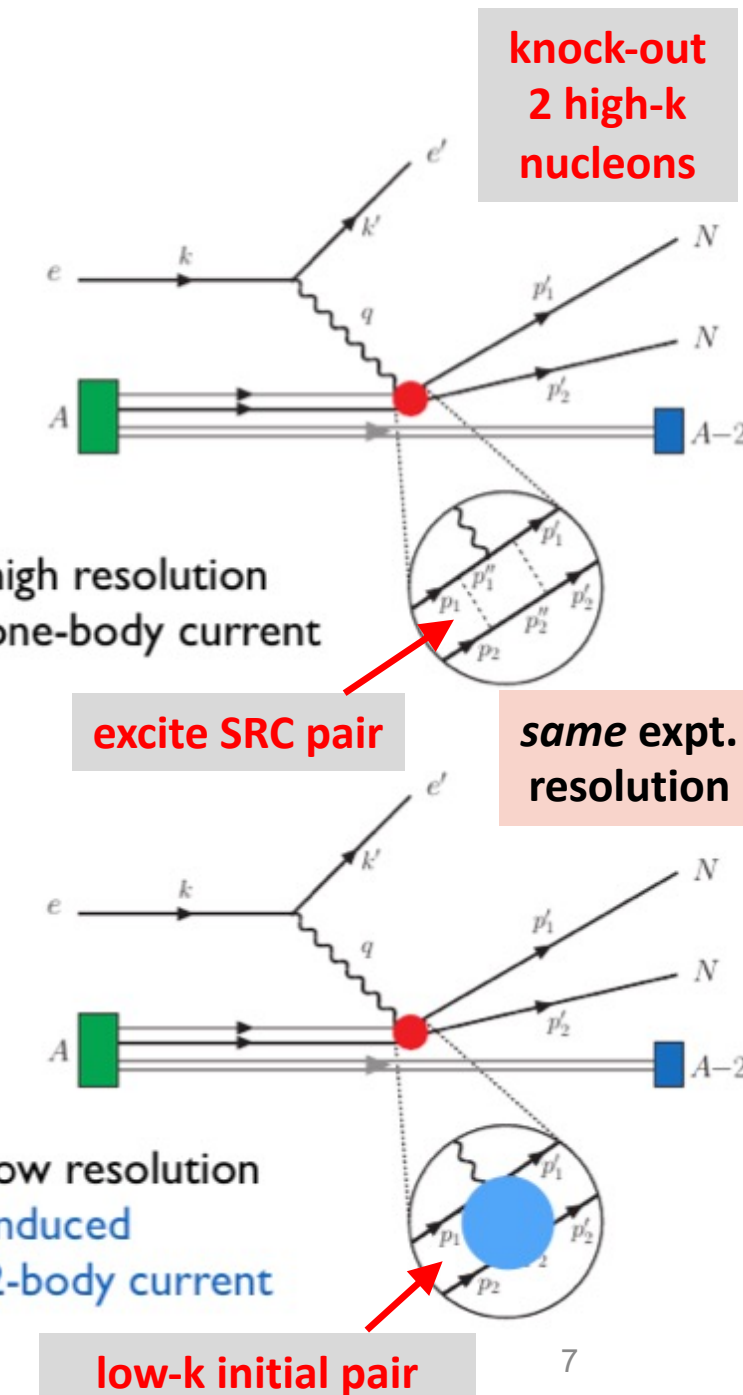
High and low RG resolution

- High RG resolution: One-body current operators with correlated wave functions
- Low RG resolution: Two-body current operators with uncorrelated wave functions
 - Operators do NOT become hard, which simplifies calculations!



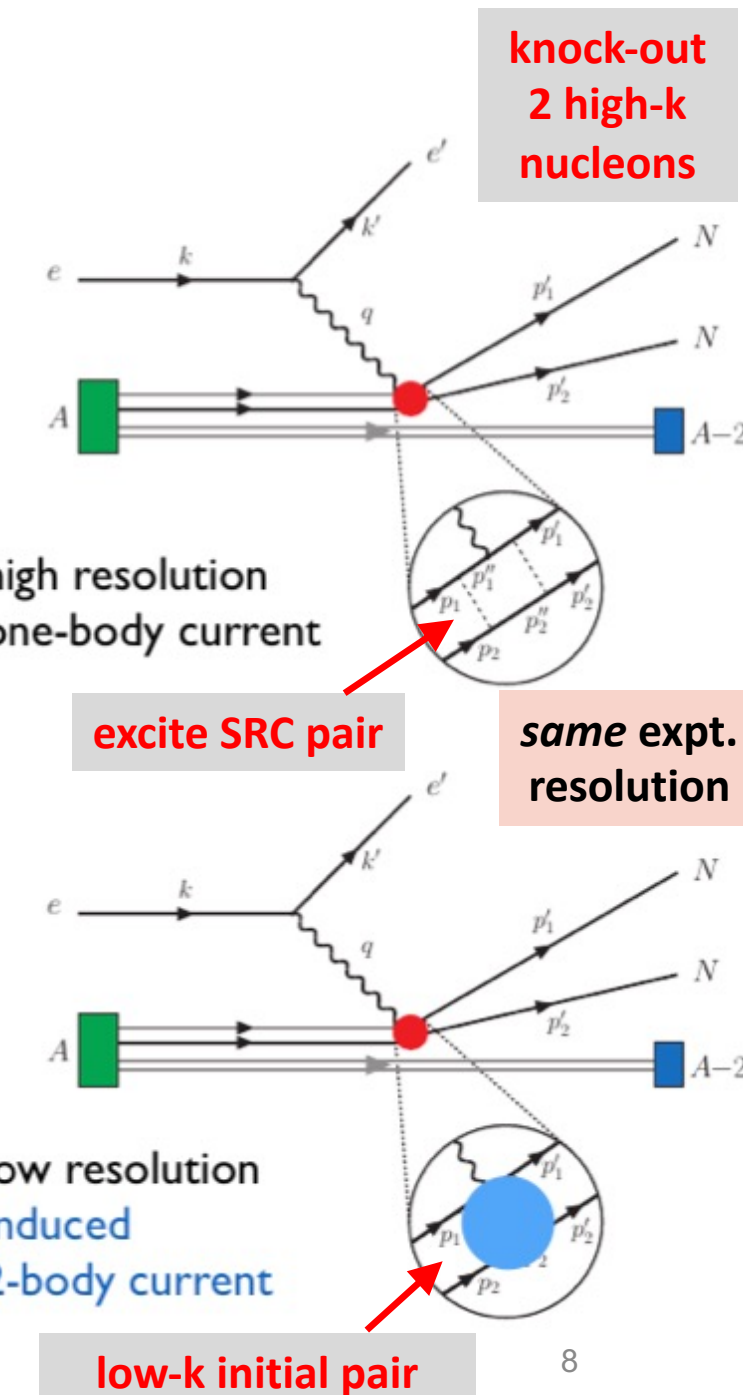
High and low RG resolution

- High RG resolution: One-body current operators with correlated wave functions
- Low RG resolution: Two-body current operators with uncorrelated wave functions
 - Operators do NOT become hard, which simplifies calculations!
- Experimental resolution (set by momentum of probe) is the same in both pictures
- Same observables but different physical interpretation!



High and low RG resolution

- High RG resolution: One-body current operators with correlated wave functions
- Low RG resolution: Two-body current operators with uncorrelated wave functions
 - Operators do NOT become hard, which simplifies calculations!
- Experimental resolution (set by momentum of probe) is the same in both pictures
- Same observables but different physical interpretation!
- This talk:
 - How can SRC calculations be carried out at low RG resolution?
 - What can we describe with simple approximations?
 - Connections to existing SRC phenomenology (e.g., GCF/LCA)



Similarity renormalization group

- Evolve to low RG resolution using the SRG

$$O(s) = U(s)O(0)U^\dagger(s)$$

where $s = 0 \rightarrow \infty$ and $U(s)$ is unitary

- SRG transformations decouple high- and low-momenta in the Hamiltonian

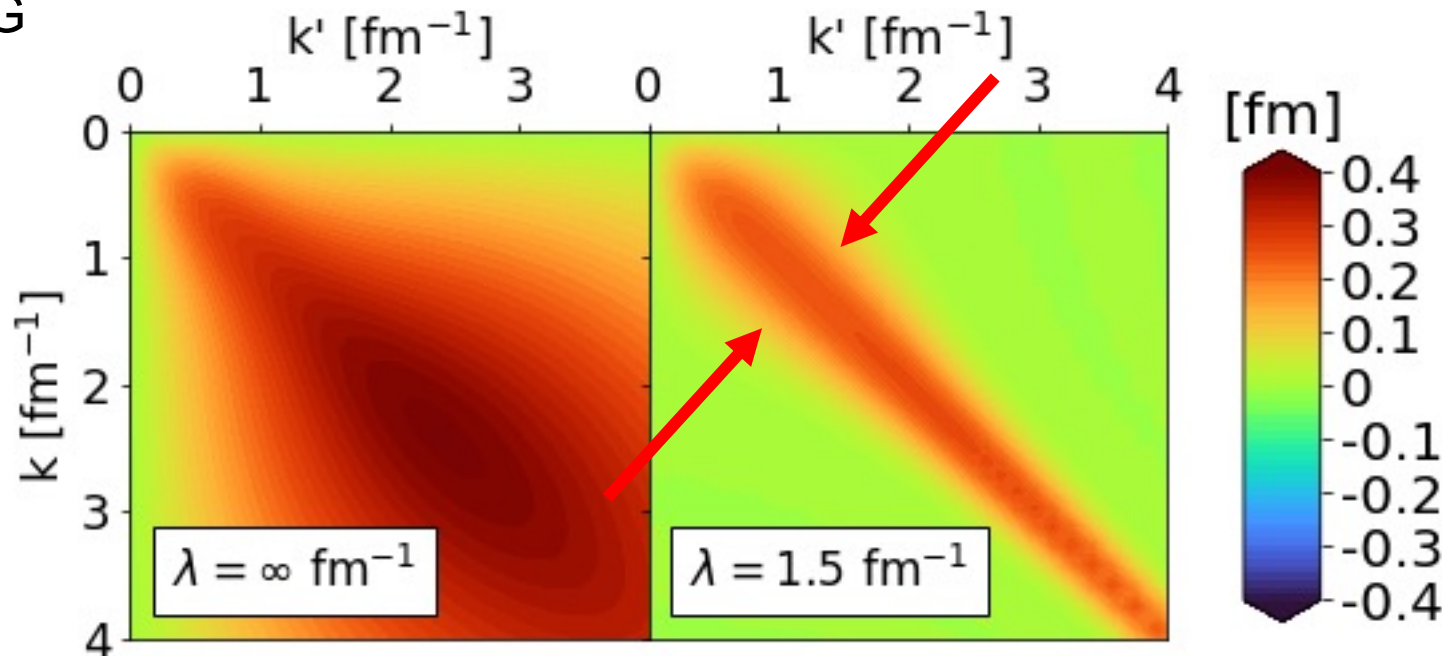


Fig. 1: Momentum space matrix elements of Argonne v18 (AV18) under SRG evolution in 1P_1 channel.

Similarity renormalization group

- Evolve to low RG resolution using the SRG

$$O(s) = U(s)O(0)U^\dagger(s)$$

where $s = 0 \rightarrow \infty$ and $U(s)$ is unitary

- SRG transformations decouple high- and low-momenta in the Hamiltonian
- In practice, solve differential flow equation

$$\frac{dO(s)}{ds} = [\eta(s), O(s)]$$

where $\eta(s) \equiv \frac{dU(s)}{ds} U^\dagger(s) = [G, H(s)]$ is the SRG generator

- Decoupling scale given by $\lambda = s^{-1/4}$

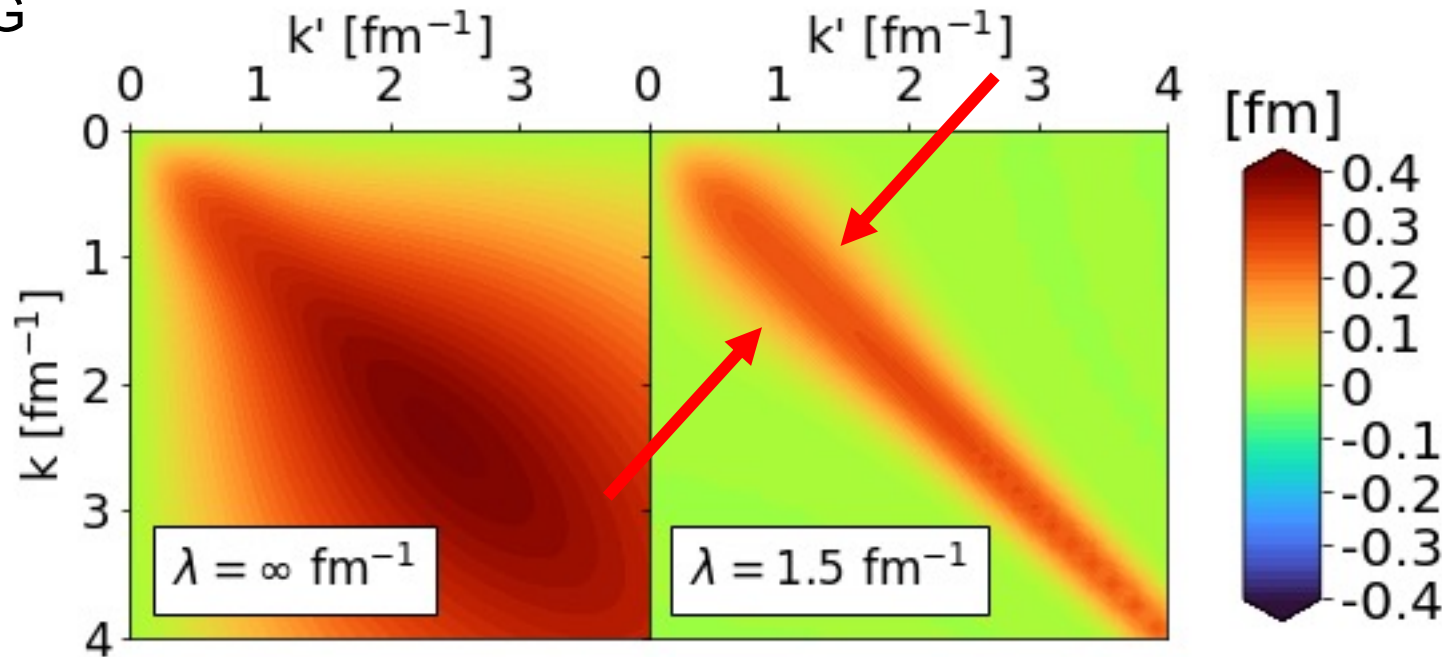


Fig. 1: Momentum space matrix elements of Argonne v18 (AV18) under SRG evolution in ${}^1\text{P}_1$ channel.

Similarity renormalization group

- AV18 wave function has significant SRC
- What happens to the wave function under SRG transformation?

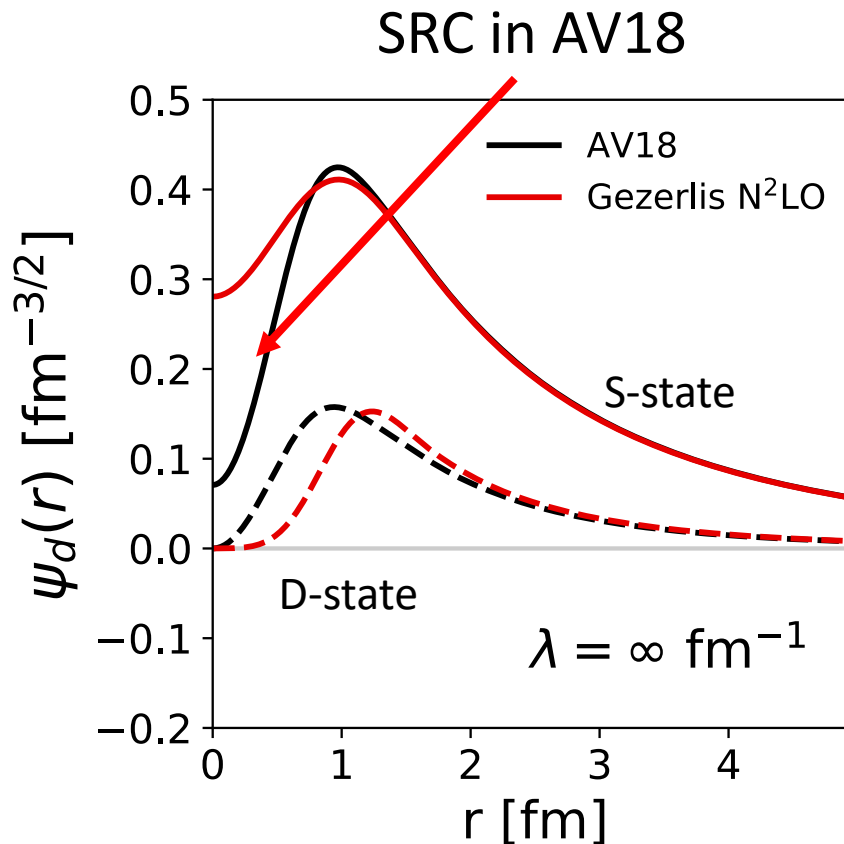


Fig. 2: SRG evolution of deuteron wave function in coordinate space for AV18 and Gezerlis $N^2\text{LO}$ ¹.

Similarity renormalization group

- SRC physics in AV18 is gone from wave function at low RG resolution
- Deuteron wave functions become soft and D-state probability goes down
- Observables such as asymptotic D-S ratio are the same

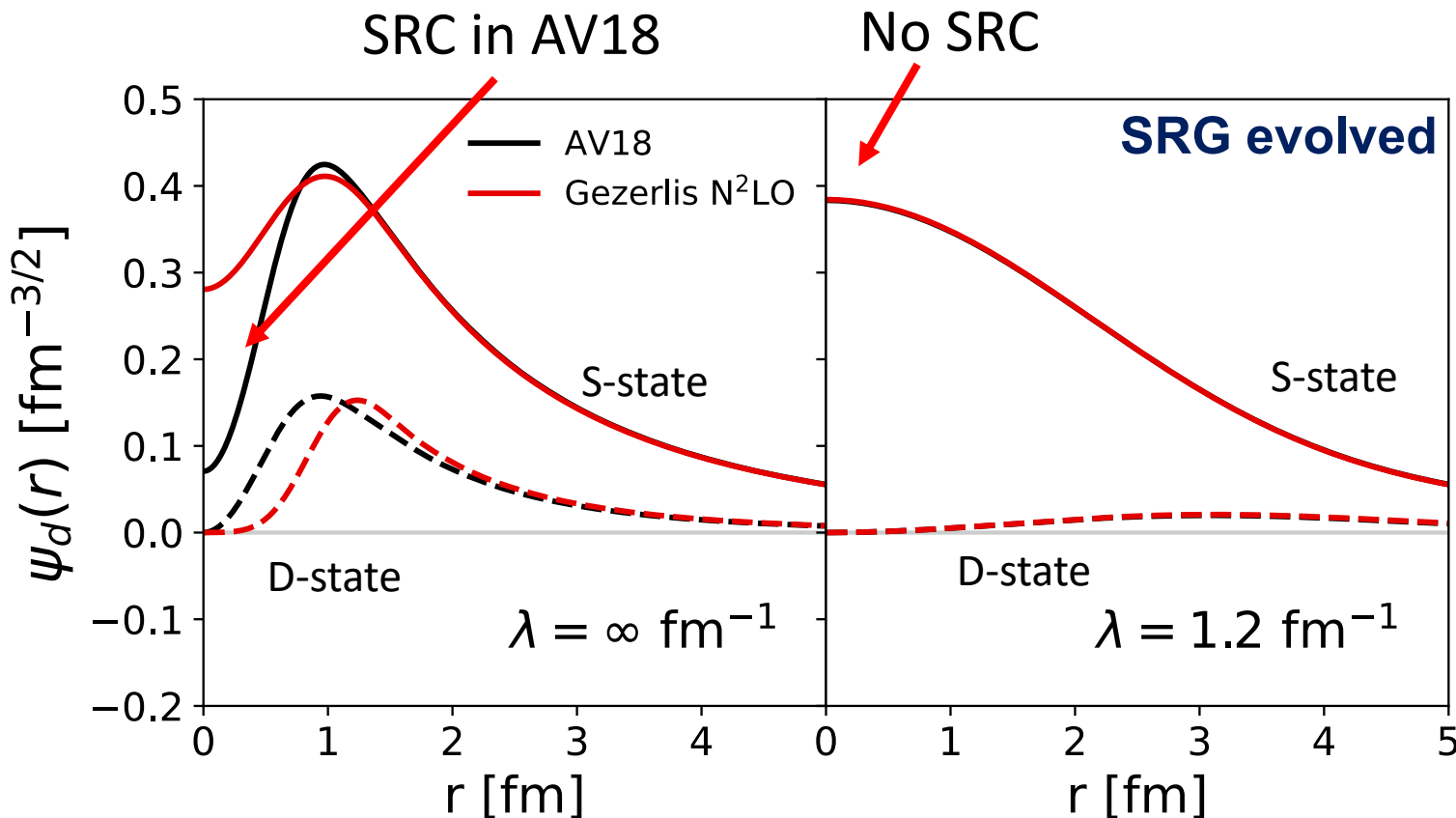


Fig. 2: SRG evolution of deuteron wave function in coordinate space for AV18 and Gezerlis N²LO¹.

Operator evolution

- Soft wave functions at low RG resolution
- SRC physics shifts to the operators

$$\langle \psi_f^{hi} | U_\lambda^\dagger U_\lambda O^{hi} U_\lambda^\dagger U_\lambda | \psi_i^{hi} \rangle = \langle \psi_f^{low} | O^{low} | \psi_i^{low} \rangle$$

Operator evolution

- Soft wave functions at low RG resolution
- SRC physics shifts to the operators

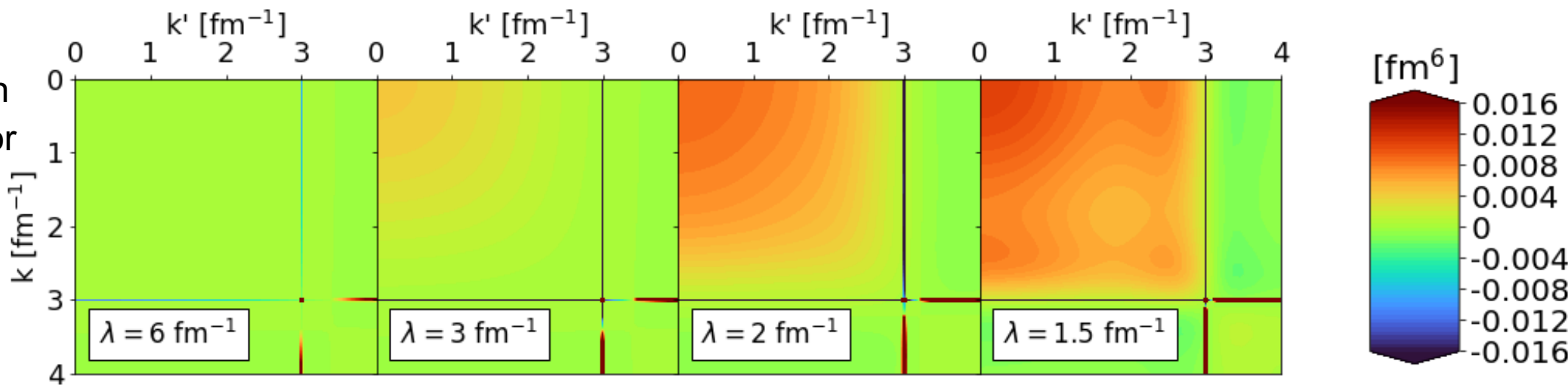
$$\langle \psi_f^{hi} | U_\lambda^\dagger U_\lambda O^{hi} U_\lambda^\dagger U_\lambda | \psi_i^{hi} \rangle = \langle \psi_f^{low} | O^{low} | \psi_i^{low} \rangle$$

- **Example:** Calculate deuteron momentum distribution by evolving momentum projection operator $a_q^\dagger a_q$

$$n_d(q) = \langle \psi_d | a_q^\dagger a_q | \psi_d \rangle = \langle \psi_d^\lambda | U_\lambda a_q^\dagger a_q U_\lambda^\dagger | \psi_d^\lambda \rangle$$

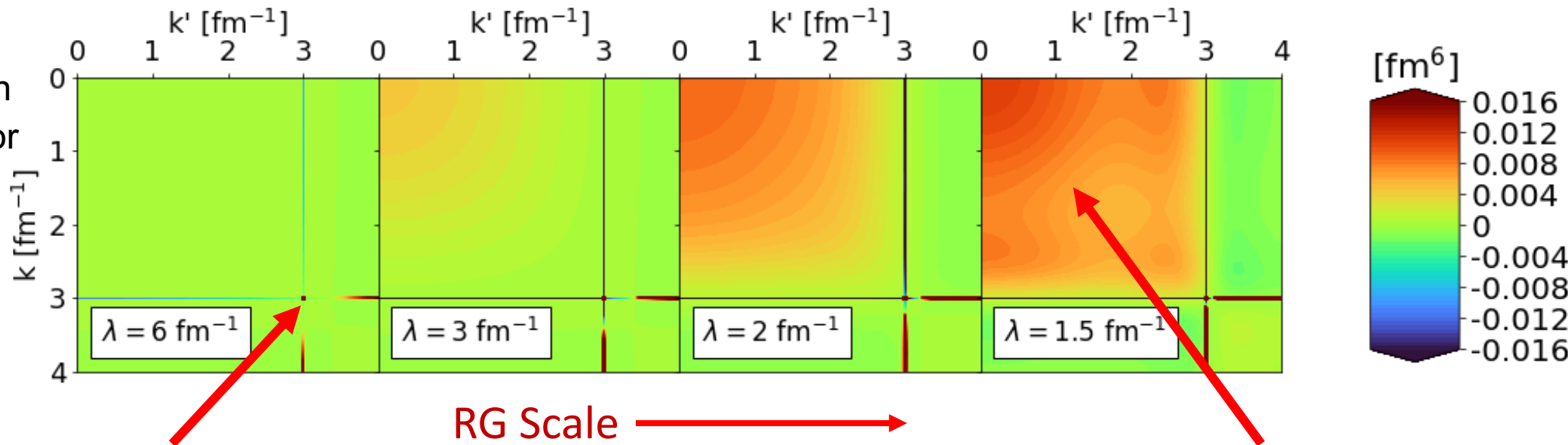
Operator evolution

Fig. 3: Evolved momentum projection operator $U_\lambda a_q^\dagger a_q U_\lambda^\dagger$ for several λ values where $q = 3 \text{ fm}^{-1}$.



Operator evolution

Fig. 3: Evolved momentum projection operator $U_\lambda a_q^\dagger a_q U_\lambda^\dagger$ for several λ values where $q = 3 \text{ fm}^{-1}$.

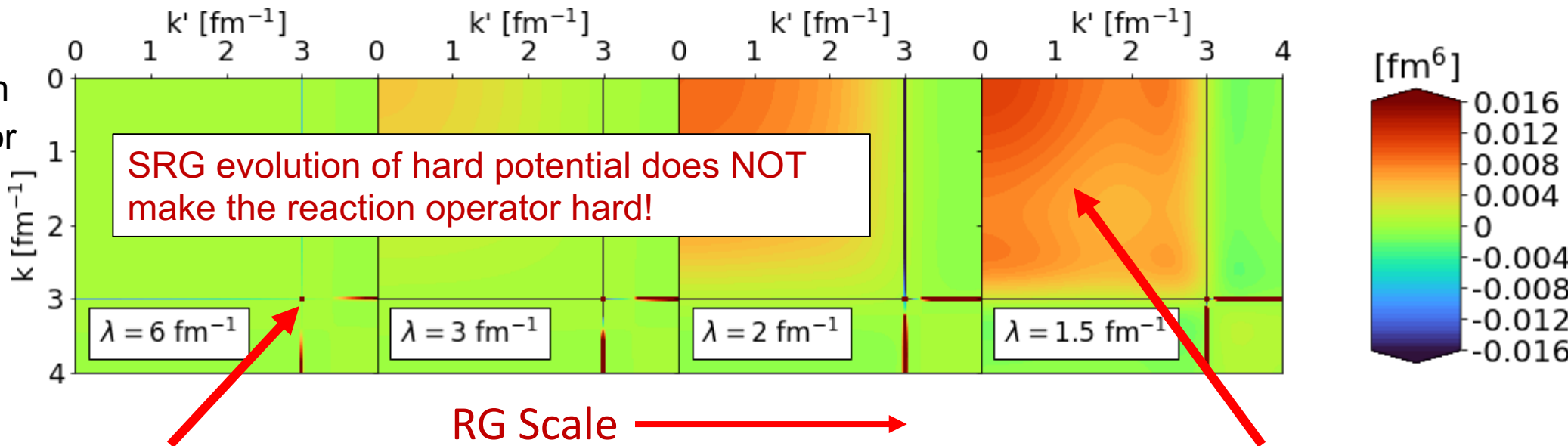


Initial operator is a discretized delta function in momentum space
 $\sim \delta(k - q)\delta(k' - q)$

SRG evolution induces smooth, low-momentum contributions

Operator evolution

Fig. 3: Evolved momentum projection operator $U_\lambda a_q^\dagger a_q U_\lambda^\dagger$ for several λ values where $q = 3 \text{ fm}^{-1}$.



Initial operator is a discretized delta function in momentum space
 $\sim \delta(k - q)\delta(k' - q)$

SRG evolution induces smooth, low-momentum contributions

Operator evolution

Fig. 3: Evolved momentum projection operator $U_\lambda a_q^\dagger a_q U_\lambda^\dagger$ for several λ values where $q = 3 \text{ fm}^{-1}$.

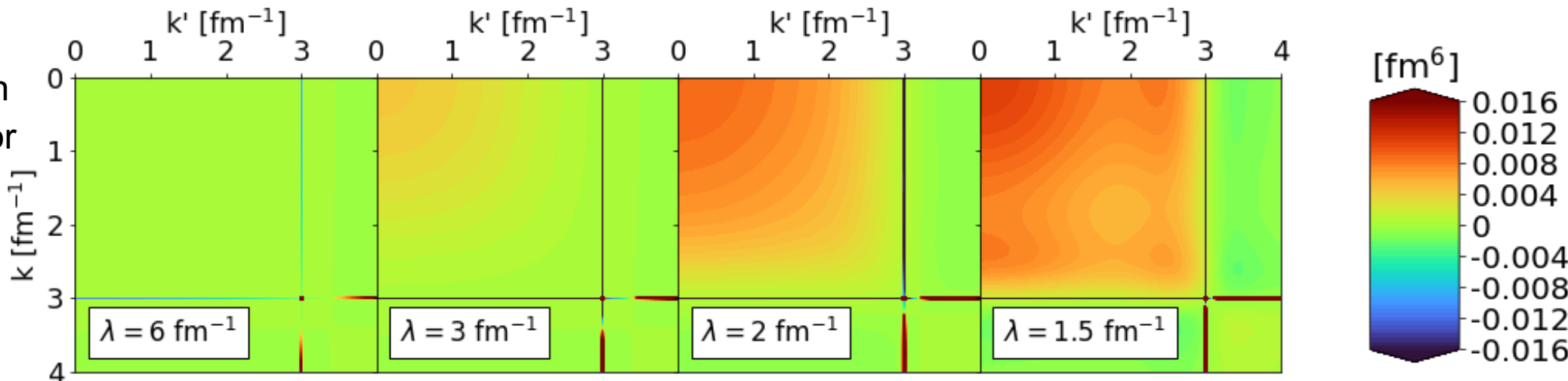
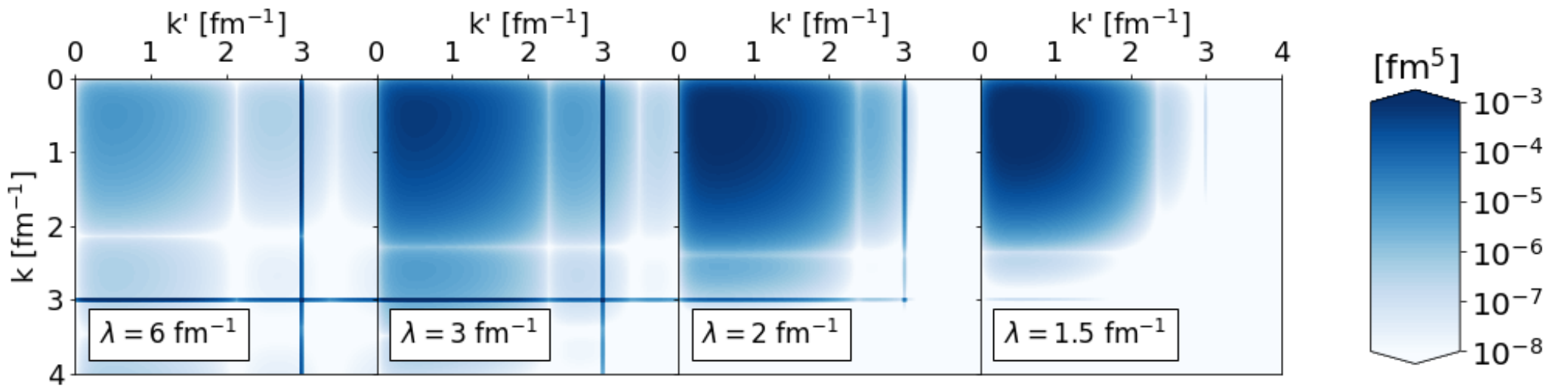


Fig. 4: Integrand of $\langle \psi_d^\lambda | U_\lambda a_q^\dagger a_q U_\lambda^\dagger | \psi_d^\lambda \rangle$ where $q = 3 \text{ fm}^{-1}$.



Operator evolution

Fig. 3: Evolved momentum projection operator $U_\lambda a_q^\dagger a_q U_\lambda^\dagger$ for several λ values where $q = 3 \text{ fm}^{-1}$.

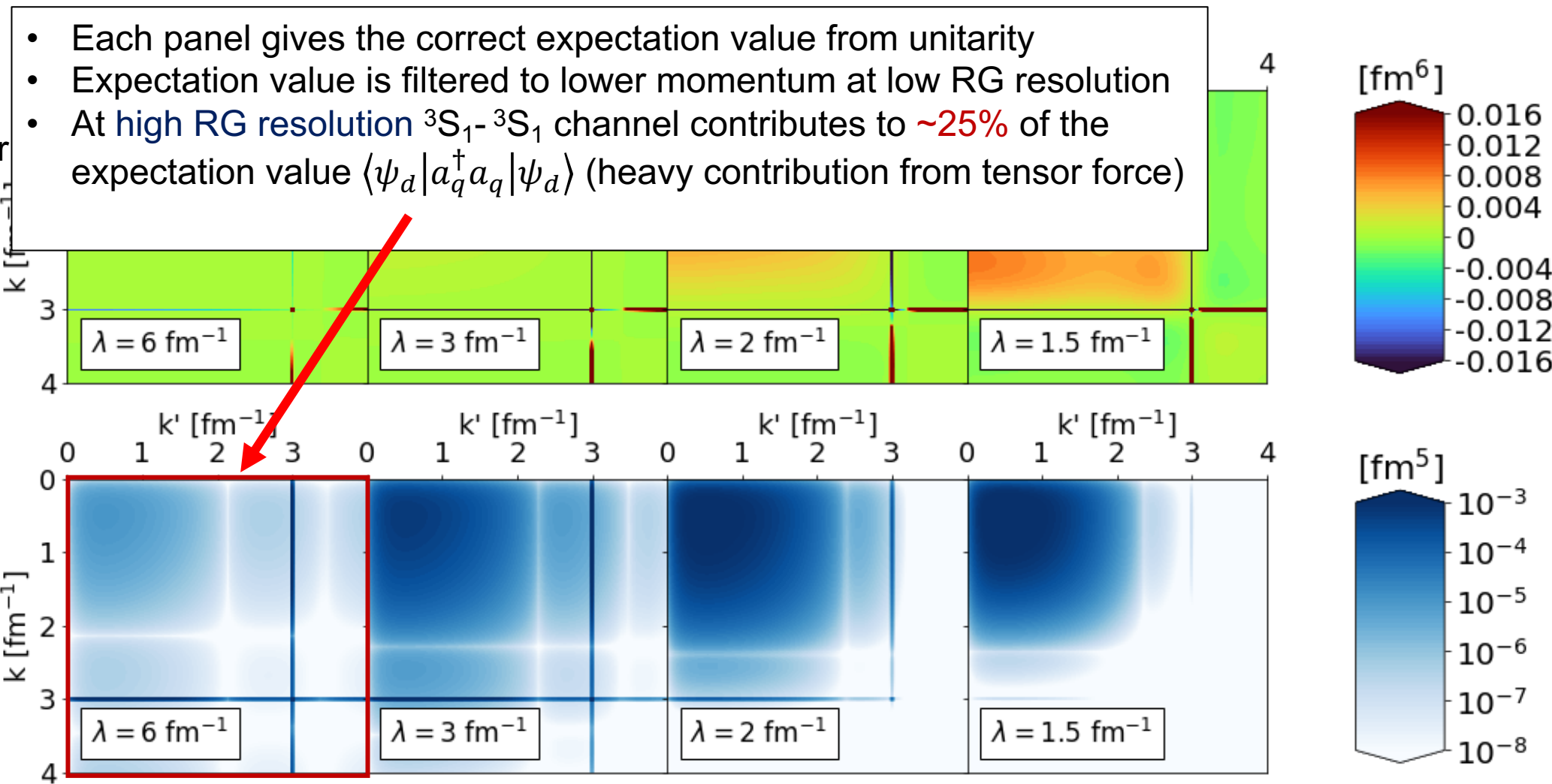


Fig. 4: Integrand of $\langle \psi_d^\lambda | U_\lambda a_q^\dagger a_q U_\lambda^\dagger | \psi_d^\lambda \rangle$ where $q = 3 \text{ fm}^{-1}$.

Operator evolution

Fig. 3: Evolved momentum projection operator $U_\lambda a_q^\dagger a_q U_\lambda^\dagger$ for several λ values where $q = 3 \text{ fm}^{-1}$.

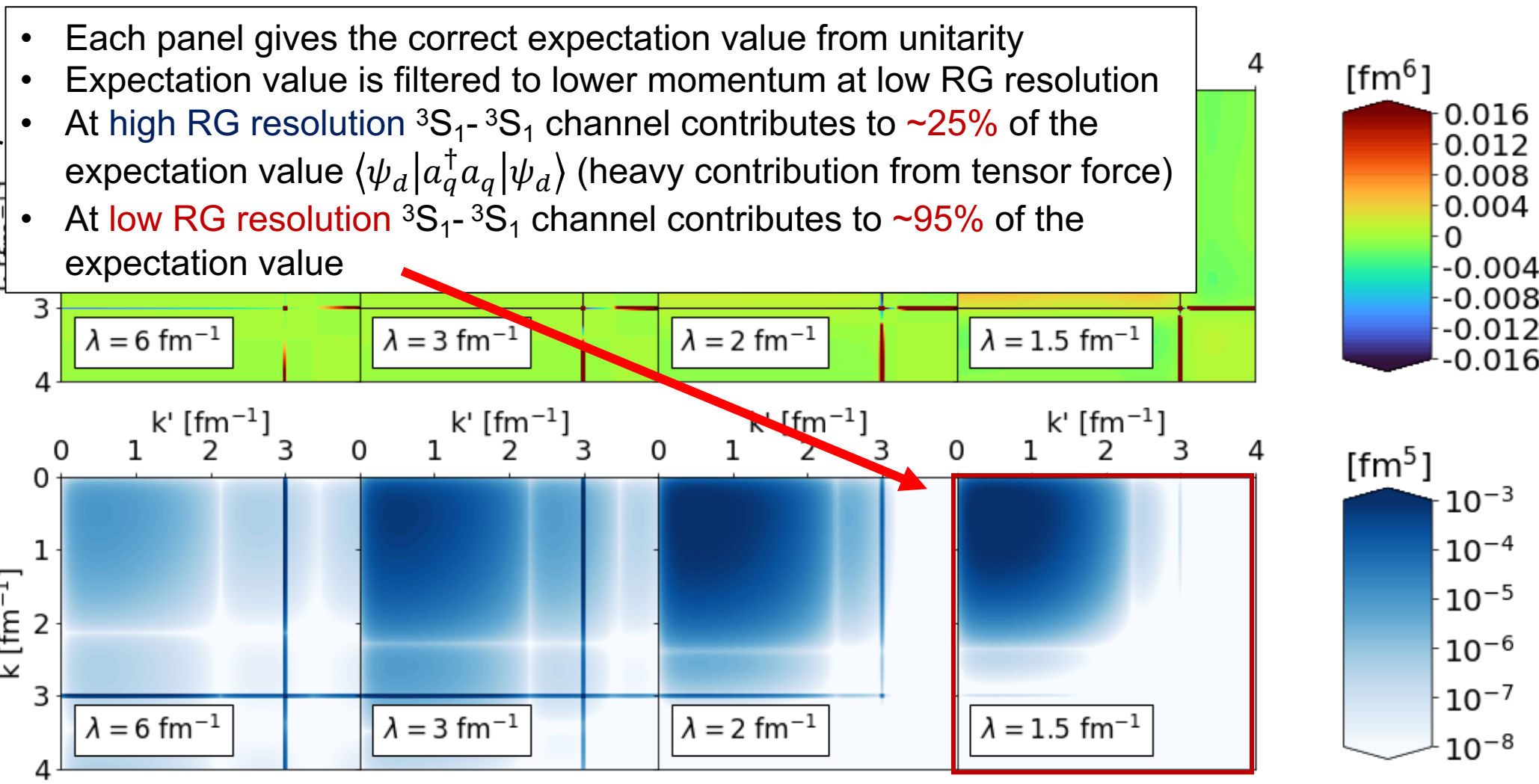


Fig. 4: Integrand of $\langle \psi_d^\lambda | U_\lambda a_q^\dagger a_q U_\lambda^\dagger | \psi_d^\lambda \rangle$ where $q = 3 \text{ fm}^{-1}$.

Momentum distributions at low RG resolution

- Apply SRG transformations to momentum distribution operators
 - Single-nucleon momentum distribution: $\hat{n}^{hi}(\mathbf{q}) = a_{\mathbf{q}}^\dagger a_{\mathbf{q}}$
 - Pair momentum distribution: $\hat{n}^{hi}(\mathbf{q}, \mathbf{Q}) = a_{\frac{\mathbf{Q}}{2}+\mathbf{q}}^\dagger a_{\frac{\mathbf{Q}}{2}-\mathbf{q}}^\dagger a_{\frac{\mathbf{Q}}{2}-\mathbf{q}} a_{\frac{\mathbf{Q}}{2}+\mathbf{q}}$

Momentum distributions at low RG resolution

- Apply SRG transformations to momentum distribution operators
 - Single-nucleon momentum distribution: $\hat{n}^{hi}(\mathbf{q}) = a_{\mathbf{q}}^\dagger a_{\mathbf{q}}$
 - Pair momentum distribution: $\hat{n}^{hi}(\mathbf{q}, \mathbf{Q}) = a_{\frac{\mathbf{Q}}{2}+\mathbf{q}}^\dagger a_{\frac{\mathbf{Q}}{2}-\mathbf{q}}^\dagger a_{\frac{\mathbf{Q}}{2}-\mathbf{q}} a_{\frac{\mathbf{Q}}{2}+\mathbf{q}}$
- Expand SRG transformation to 2-body level

$$\widehat{U}_\lambda = 1 + \frac{1}{4} \sum_{\mathbf{K}, \mathbf{k}, \mathbf{k}'} \delta U_\lambda^{(2)}(\mathbf{k}, \mathbf{k}') a_{\frac{\mathbf{K}}{2}+\mathbf{k}}^\dagger a_{\frac{\mathbf{K}}{2}-\mathbf{k}}^\dagger a_{\frac{\mathbf{K}}{2}-\mathbf{k}'} a_{\frac{\mathbf{K}}{2}+\mathbf{k}'} + \dots$$

- $\delta U_\lambda^{(2)}$ term is fixed by SRG evolution on $A = 2$ and inherits the symmetries of V_{NN}

Momentum distributions at low RG resolution

- Apply SRG transformations to momentum distribution operators
 - Single-nucleon momentum distribution: $\hat{n}^{hi}(\mathbf{q}) = a_{\mathbf{q}}^\dagger a_{\mathbf{q}}$
 - Pair momentum distribution: $\hat{n}^{hi}(\mathbf{q}, \mathbf{Q}) = a_{\frac{\mathbf{Q}}{2}+\mathbf{q}}^\dagger a_{\frac{\mathbf{Q}}{2}-\mathbf{q}}^\dagger a_{\frac{\mathbf{Q}}{2}-\mathbf{q}} a_{\frac{\mathbf{Q}}{2}+\mathbf{q}}$
- Expand SRG transformation to 2-body level

$$\hat{U}_\lambda = 1 + \frac{1}{4} \sum_{\mathbf{K}, \mathbf{k}, \mathbf{k}'} \delta U_\lambda^{(2)}(\mathbf{k}, \mathbf{k}') a_{\frac{\mathbf{K}}{2}+\mathbf{k}}^\dagger a_{\frac{\mathbf{K}}{2}-\mathbf{k}}^\dagger a_{\frac{\mathbf{K}}{2}-\mathbf{k}'} a_{\frac{\mathbf{K}}{2}+\mathbf{k}'} + \dots$$

- $\delta U_\lambda^{(2)}$ term is fixed by SRG evolution on $A = 2$ and inherits the symmetries of V_{NN}
- **Strategy:** Apply Wick's theorem to evaluate $\hat{U}_\lambda \hat{n}^{hi}(\mathbf{q}) \hat{U}_\lambda^\dagger$ and $\hat{U}_\lambda \hat{n}^{hi}(\mathbf{q}, \mathbf{Q}) \hat{U}_\lambda^\dagger$ truncating 3-body and higher terms

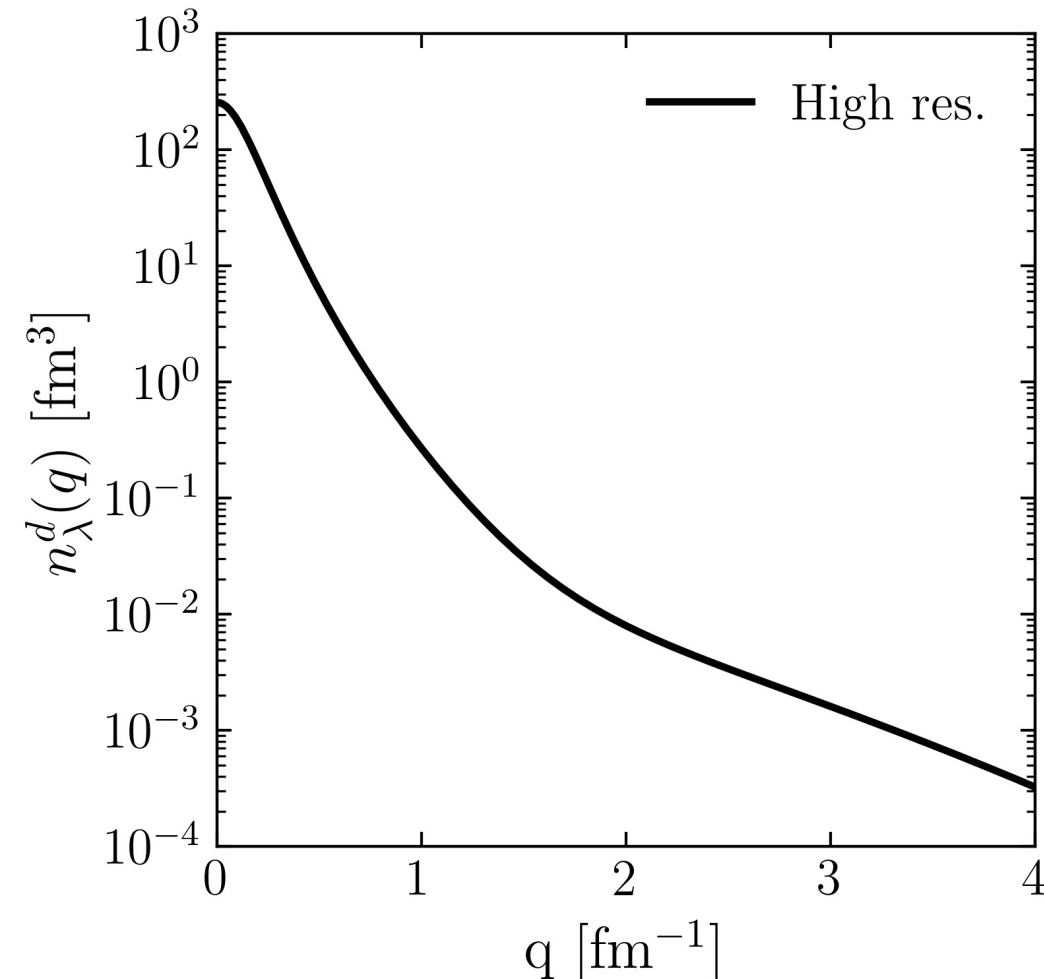
Momentum distributions at low RG resolution

- **Example:** Evolved single-nucleon momentum distribution

$$\begin{aligned} & \widehat{U}_\lambda \widehat{n}^{hi}(\mathbf{q}) \widehat{U}_\lambda^\dagger \\ & \approx a_{\mathbf{q}}^\dagger a_{\mathbf{q}} + \frac{1}{2} \sum_{\mathbf{K}, \mathbf{k}} [\delta U_\lambda^{(2)} \left(\mathbf{k}, \mathbf{q} - \frac{\mathbf{K}}{2} \right) a_{\frac{\mathbf{K}}{2} + \mathbf{k}}^\dagger a_{\frac{\mathbf{K}}{2} - \mathbf{k}}^\dagger a_{\mathbf{K} - \mathbf{q}} a_{\mathbf{q}} + \delta U_\lambda^{\dagger(2)} \left(\mathbf{q} - \frac{\mathbf{K}}{2}, \mathbf{k} \right) a_{\mathbf{q}}^\dagger a_{\mathbf{K} - \mathbf{q}}^\dagger a_{\frac{\mathbf{K}}{2} - \mathbf{k}}^\dagger a_{\frac{\mathbf{K}}{2} + \mathbf{k}}] \\ & + \frac{1}{4} \sum_{\mathbf{K}, \mathbf{k}, \mathbf{k}'} \delta U_\lambda^{(2)} \left(\mathbf{k}, \mathbf{q} - \frac{\mathbf{K}}{2} \right) \delta U_\lambda^{\dagger(2)} \left(\mathbf{q} - \frac{\mathbf{K}}{2}, \mathbf{k}' \right) a_{\frac{\mathbf{K}}{2} + \mathbf{k}}^\dagger a_{\frac{\mathbf{K}}{2} - \mathbf{k}}^\dagger a_{\frac{\mathbf{K}}{2} - \mathbf{k}'}^\dagger a_{\frac{\mathbf{K}}{2} + \mathbf{k}'} \end{aligned}$$

- For operator that probes high momentum ($q \gg \lambda$), the low RG resolution wave function filters out first few terms leaving only $\delta U \delta U^\dagger$ term

Momentum distributions at low RG resolution



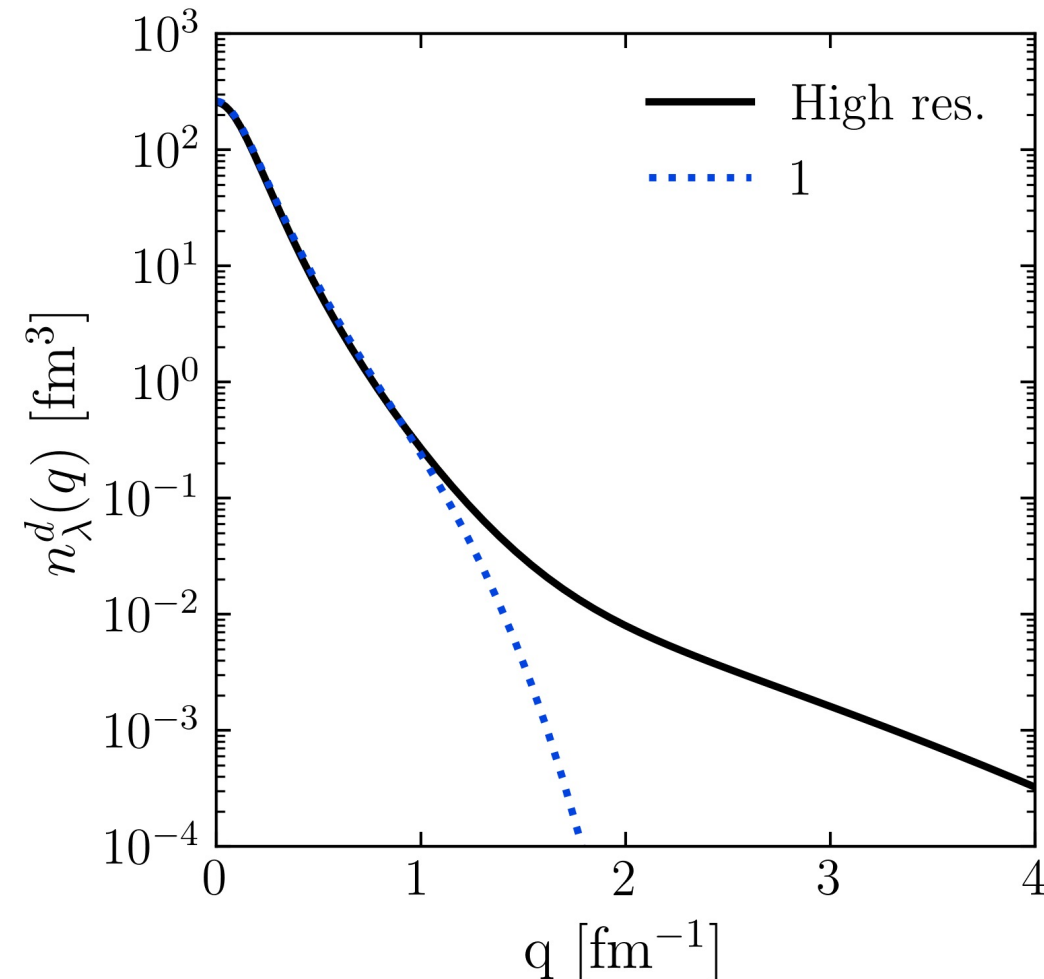
- Deuteron example

$$n^{lo}(\mathbf{q}) = (1 + \delta U) a_{\mathbf{q}}^\dagger a_{\mathbf{q}} (1 + \delta U^\dagger)$$

$$\langle \psi_d^{hi} | a_{\mathbf{q}}^\dagger a_{\mathbf{q}} | \psi_d^{hi} \rangle$$

Fig. 5: Contributions to deuteron momentum distribution with AV18 and $\lambda = 1.35$ fm⁻¹.

Momentum distributions at low RG resolution



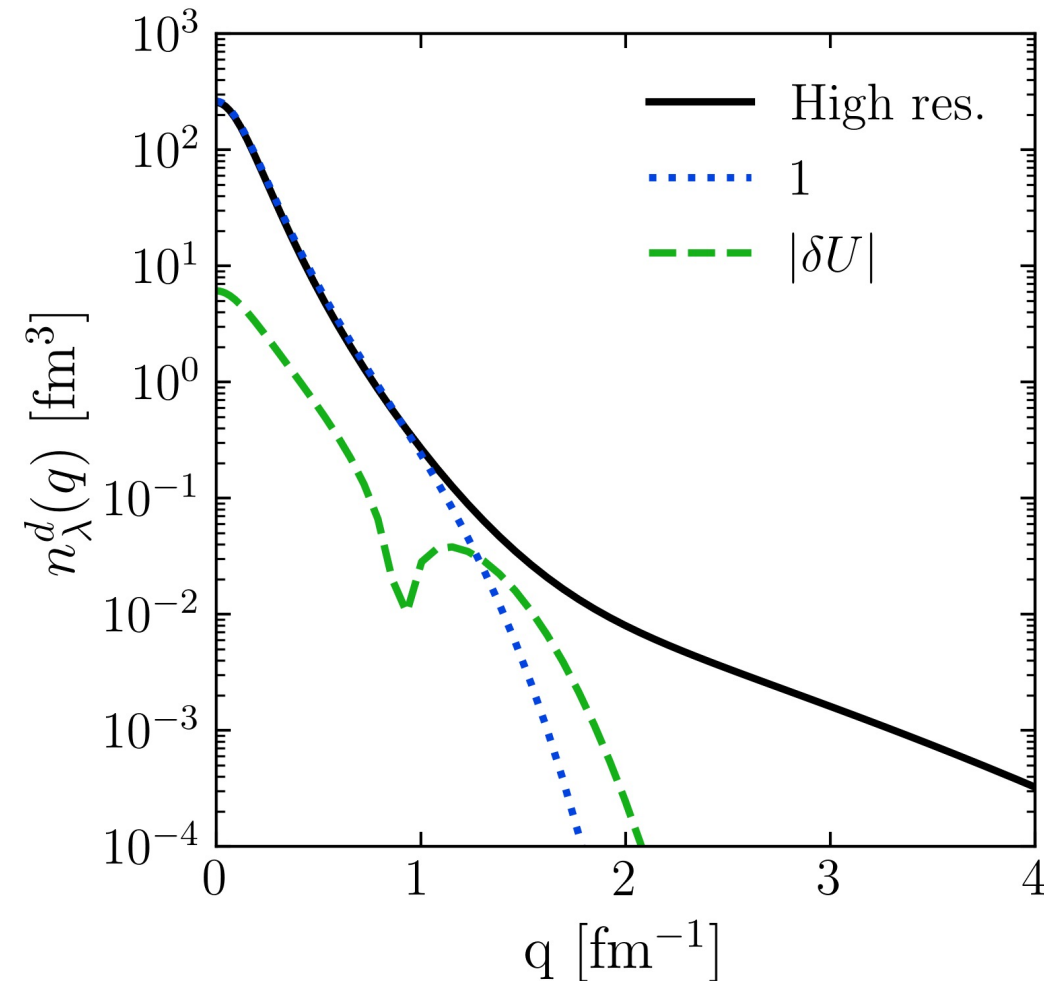
- Deuteron example

$$n^{lo}(\mathbf{q}) = (1 + \delta U) a_{\mathbf{q}}^\dagger a_{\mathbf{q}} (1 + \delta U^\dagger)$$

$$\begin{aligned}\langle \psi_d^{hi} | a_{\mathbf{q}}^\dagger a_{\mathbf{q}} | \psi_d^{hi} \rangle \\ \langle \psi_d^{lo} | a_{\mathbf{q}}^\dagger a_{\mathbf{q}} | \psi_d^{lo} \rangle\end{aligned}$$

Fig. 5: Contributions to deuteron momentum distribution with AV18 and $\lambda = 1.35 \text{ fm}^{-1}$.

Momentum distributions at low RG resolution



- Deuteron example

$$n^{lo}(\mathbf{q}) = (1 + \delta U) a_{\mathbf{q}}^\dagger a_{\mathbf{q}} (1 + \delta U^\dagger)$$

$$\langle \psi_d^{hi} | a_{\mathbf{q}}^\dagger a_{\mathbf{q}} | \psi_d^{hi} \rangle$$

$$\langle \psi_d^{lo} | a_{\mathbf{q}}^\dagger a_{\mathbf{q}} | \psi_d^{lo} \rangle$$

$$\langle \psi_d^{lo} | \delta U a_{\mathbf{q}}^\dagger a_{\mathbf{q}} + a_{\mathbf{q}}^\dagger a_{\mathbf{q}} \delta U^\dagger | \psi_d^{lo} \rangle$$

Fig. 5: Contributions to deuteron momentum distribution with AV18 and $\lambda = 1.35$ fm⁻¹.

Momentum distributions at low RG resolution

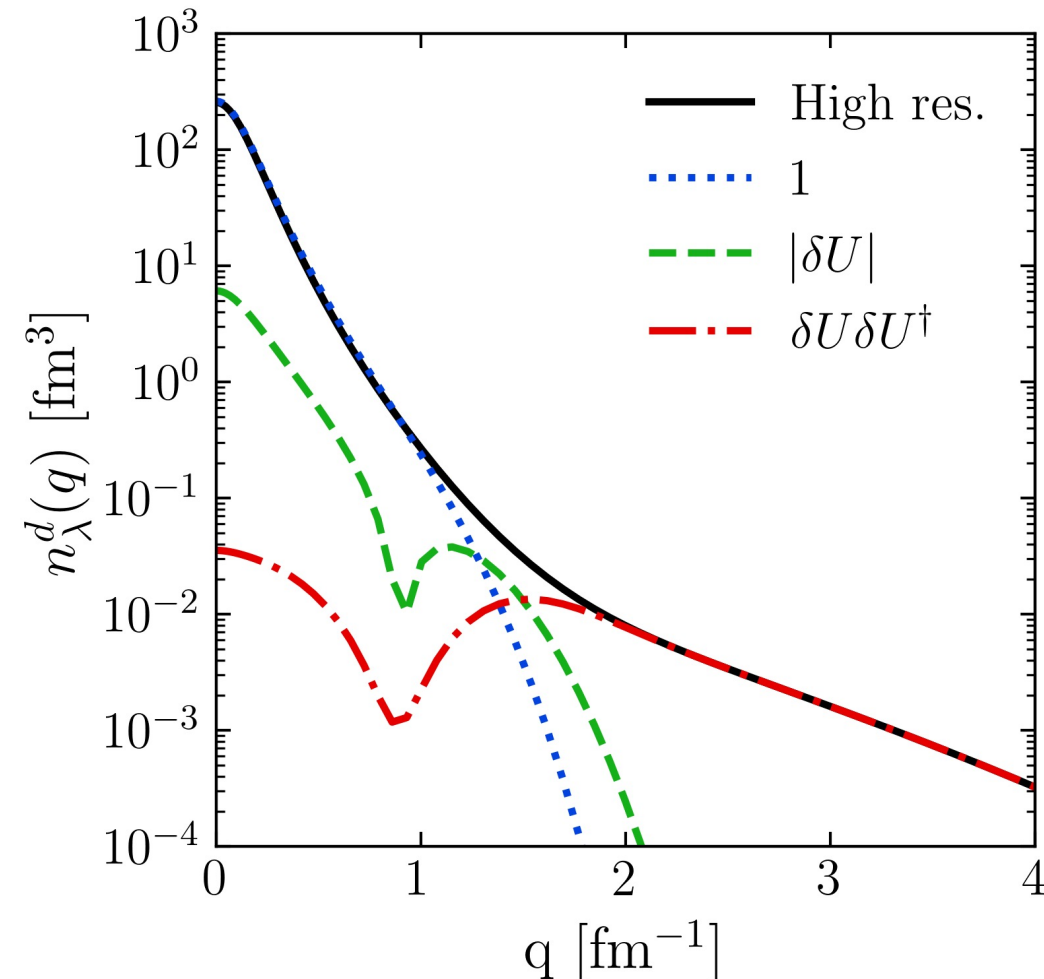


Fig. 5: Contributions to deuteron momentum distribution with AV18 and $\lambda = 1.35 \text{ fm}^{-1}$.

- Deuteron example

$$n^{lo}(\mathbf{q}) = (1 + \delta U) a_{\mathbf{q}}^\dagger a_{\mathbf{q}} (1 + \delta U^\dagger)$$

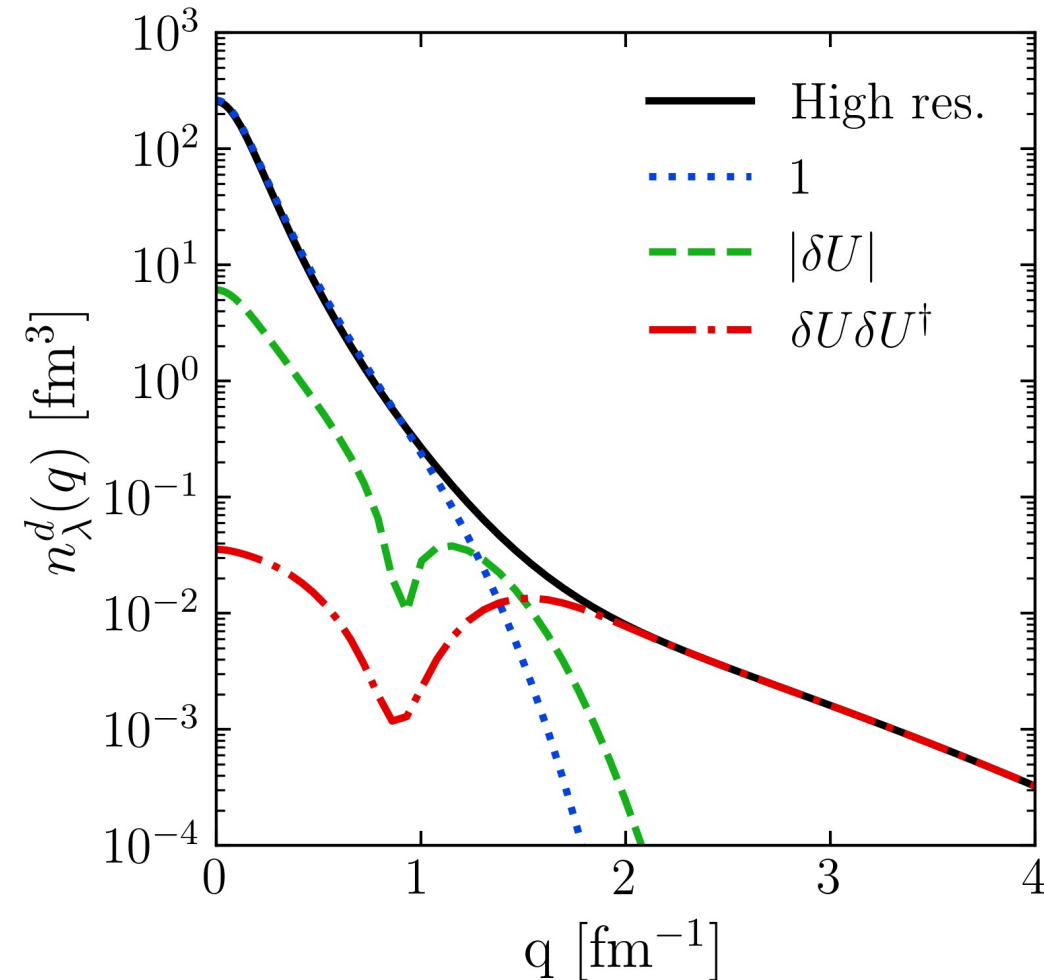
$$\langle \psi_d^{hi} | a_{\mathbf{q}}^\dagger a_{\mathbf{q}} | \psi_d^{hi} \rangle$$

$$\langle \psi_d^{lo} | a_{\mathbf{q}}^\dagger a_{\mathbf{q}} | \psi_d^{lo} \rangle$$

$$\langle \psi_d^{lo} | \delta U a_{\mathbf{q}}^\dagger a_{\mathbf{q}} + a_{\mathbf{q}}^\dagger a_{\mathbf{q}} \delta U^\dagger | \psi_d^{lo} \rangle$$

$$\langle \psi_d^{lo} | \delta U a_{\mathbf{q}}^\dagger a_{\mathbf{q}} \delta U^\dagger | \psi_d^{lo} \rangle$$

Momentum distributions at low RG resolution

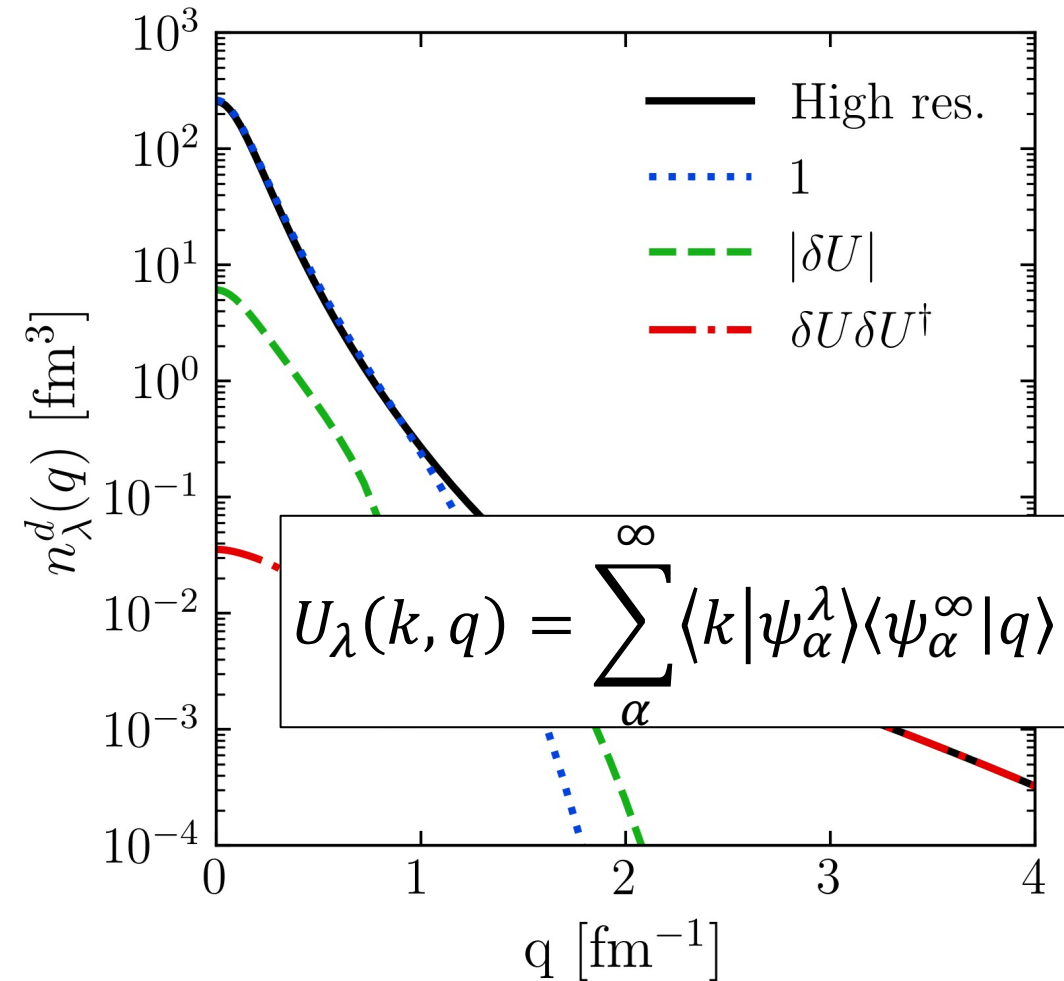


- For high- q , the $\delta U_\lambda \delta U_\lambda^\dagger$ term dominates

$$\approx \sum_{K,k,k'}^{\lambda} \delta U_\lambda(\mathbf{k}, \mathbf{q}) \delta U_\lambda^\dagger(\mathbf{q}, \mathbf{k}') a_{\frac{\mathbf{K}}{2}+\mathbf{k}}^\dagger a_{\frac{\mathbf{K}}{2}-\mathbf{k}}^\dagger a_{\frac{\mathbf{K}}{2}-\mathbf{k}'} a_{\frac{\mathbf{K}}{2}+\mathbf{k}'}$$

Fig. 5: Contributions to deuteron momentum distribution with AV18 and $\lambda = 1.35 \text{ fm}^{-1}$.

Momentum distributions at low RG resolution



- For high- q , the $\delta U_\lambda \delta U_\lambda^\dagger$ term dominates

$$\approx \sum_{K, k, k'}^{\lambda} \delta U_\lambda(\mathbf{k}, q) \delta U_\lambda^\dagger(\mathbf{q}, \mathbf{k}') a_{\frac{\mathbf{K}}{2} + \mathbf{k}}^\dagger a_{\frac{\mathbf{K}}{2} - \mathbf{k}}^\dagger a_{\frac{\mathbf{K}}{2} - \mathbf{k}'} a_{\frac{\mathbf{K}}{2} + \mathbf{k}'}$$

→ **Factorization:** $\delta U_\lambda(\mathbf{k}, q) \approx F_\lambda^{lo}(\mathbf{k}) F_\lambda^{hi}(q)$

$$\approx |F_\lambda^{hi}(q)|^2 \sum_{K, k, k'}^{\lambda} F_\lambda^{lo}(\mathbf{k}) F_\lambda^{lo}(\mathbf{k}') a_{\frac{\mathbf{K}}{2} + \mathbf{k}}^\dagger a_{\frac{\mathbf{K}}{2} - \mathbf{k}}^\dagger a_{\frac{\mathbf{K}}{2} - \mathbf{k}'} a_{\frac{\mathbf{K}}{2} + \mathbf{k}'}$$

Fig. 5: Contributions to deuteron momentum distribution with AV18 and $\lambda = 1.35$ fm⁻¹.

Factorization

- Factorization of SRG transformations imply scaling of high- q tails

- Consider ratio $\frac{n^A(\mathbf{q})}{n^d(\mathbf{q})}$ for $q \gg \lambda$,

$$\frac{\langle \Psi_\lambda^A | U_\lambda a_q^\dagger a_q U_\lambda^\dagger | \Psi_\lambda^A \rangle}{\langle \Psi_\lambda^d | U_\lambda a_q^\dagger a_q U_\lambda^\dagger | \Psi_\lambda^d \rangle} = \frac{|F_\lambda^{hi}(\mathbf{q})|^2}{|F_\lambda^{hi}(\mathbf{q})|^2} \times \frac{\langle \Psi_\lambda^A | \sum_{\mathbf{K}, \mathbf{k}, \mathbf{k}'} F_\lambda^{lo}(\mathbf{k}) F_\lambda^{lo}(\mathbf{k}') a_{\frac{\mathbf{K}}{2} + \mathbf{k}}^\dagger a_{\frac{\mathbf{K}}{2} - \mathbf{k}}^\dagger a_{\frac{\mathbf{K}}{2} - \mathbf{k}'} a_{\frac{\mathbf{K}}{2} + \mathbf{k}'} | \Psi_\lambda^A \rangle}{\langle \Psi_\lambda^d | \sum_{\mathbf{K}, \mathbf{k}, \mathbf{k}'} F_\lambda^{lo}(\mathbf{k}) F_\lambda^{lo}(\mathbf{k}') a_{\frac{\mathbf{K}}{2} + \mathbf{k}}^\dagger a_{\frac{\mathbf{K}}{2} - \mathbf{k}}^\dagger a_{\frac{\mathbf{K}}{2} - \mathbf{k}'} a_{\frac{\mathbf{K}}{2} + \mathbf{k}'} | \Psi_\lambda^d \rangle}$$

~~$|F_\lambda^{hi}(\mathbf{q})|^2$~~

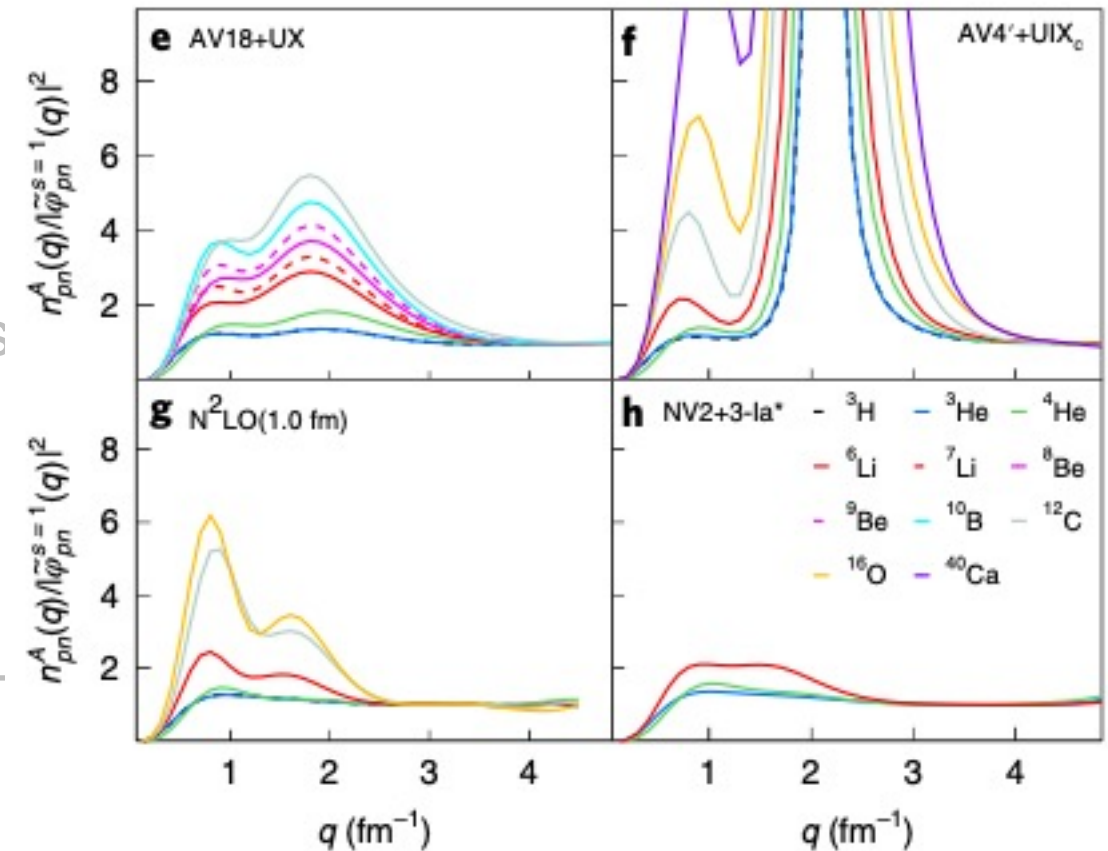
- High- q dependence cancels leaving ratio only sensitive to low-momentum physics

Factorization

- Factorization of SRG transformations imply s

Factorization built into GCF model seen by flat ratio of pair momentum distributions $n^A(q)$ over universal two-body wave functions $|\tilde{\varphi}(q)|^2$ at high- q

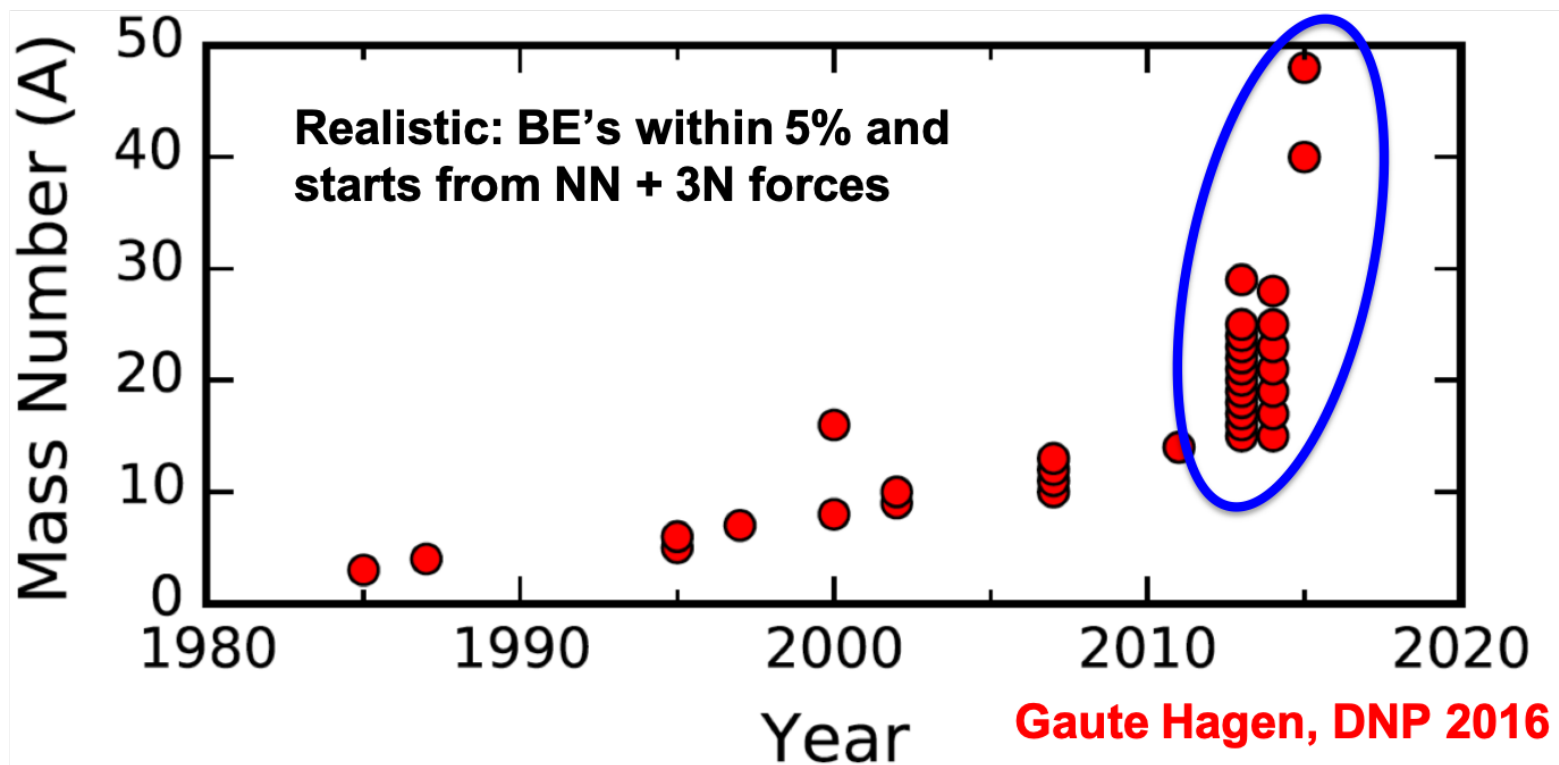
Figure from R. Cruz-Torres et al., Nat. Phys. 17, 306 (2021)



- High- q dependence cancels leaving ratio only sensitive to low-momentum physics

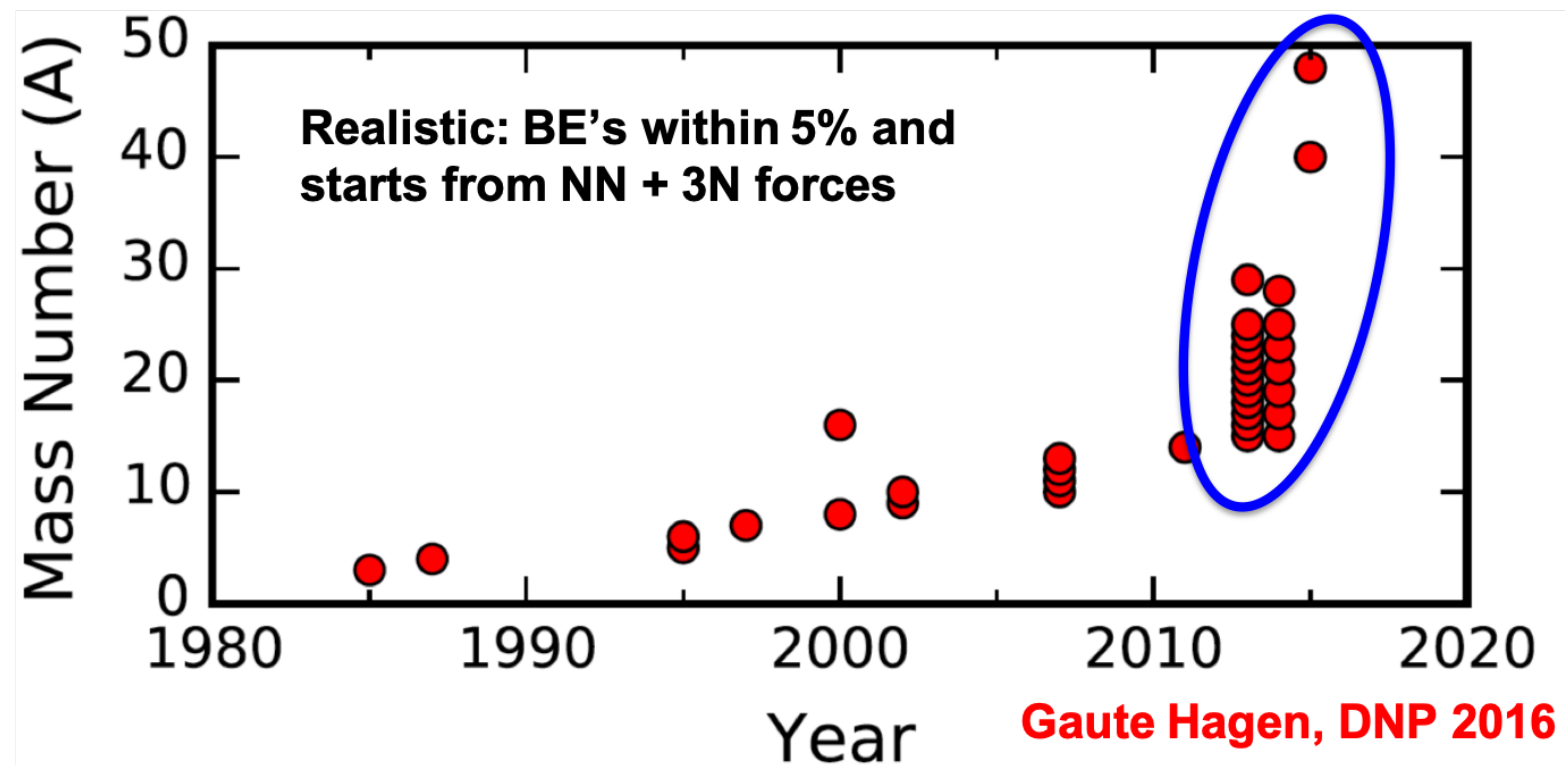
Why low RG resolution?

- Methods that rely on soft interactions work well!



Why low RG resolution?

- Methods that rely on soft interactions work well!
- What SRC physics can we describe using simple approximations?
- Try Hartree-Fock (HF) with a local density approximation (LDA) to evaluate nuclear matrix elements



HF and LDA calculation

- Evaluating SRG-evolved operator with low RG resolution wave functions $\langle \Psi_\lambda^A | \hat{U}_\lambda \hat{n}^{hi}(\mathbf{q}) \hat{U}_\lambda^\dagger | \Psi_\lambda^A \rangle$

$$\begin{aligned} &\approx \langle \Psi_\lambda^A | \left[a_{\mathbf{q}}^\dagger a_{\mathbf{q}} + \frac{1}{2} \sum_{\mathbf{K}, \mathbf{k}} \left(\delta U_\lambda(\mathbf{k}, \mathbf{q} - \mathbf{K}/2) a_{\mathbf{K}/2+\mathbf{k}}^\dagger a_{\mathbf{K}/2-\mathbf{k}}^\dagger a_{\mathbf{K}-\mathbf{q}} a_{\mathbf{q}} \right. \right. \\ &\quad \left. \left. + \delta U_\lambda^\dagger(\mathbf{q} - \mathbf{K}/2, \mathbf{k}) a_{\mathbf{q}}^\dagger a_{\mathbf{K}-\mathbf{q}}^\dagger a_{\mathbf{K}/2-\mathbf{k}} a_{\mathbf{K}/2+\mathbf{k}} \right) \right. \\ &\quad \left. + \frac{1}{4} \sum_{\mathbf{K}, \mathbf{k}, \mathbf{k}'} \delta U_\lambda(\mathbf{k}, \mathbf{q} - \mathbf{K}/2) \delta U_\lambda^\dagger(\mathbf{q} - \mathbf{K}/2, \mathbf{k}') a_{\mathbf{K}/2+\mathbf{k}}^\dagger a_{\mathbf{K}/2-\mathbf{k}}^\dagger a_{\mathbf{K}/2-\mathbf{k}'} a_{\mathbf{K}/2+\mathbf{k}'} \right] | \Psi_\lambda^A \rangle \end{aligned}$$

HF and LDA calculation

- Evaluating SRG-evolved operator with low RG resolution wave functions $\langle \Psi_\lambda^A | \hat{U}_\lambda \hat{n}^{hi}(\mathbf{q}) \hat{U}_\lambda^\dagger | \Psi_\lambda^A \rangle$

$$\begin{aligned} &\approx \langle \Psi_\lambda^A | \left[a_{\mathbf{q}}^\dagger a_{\mathbf{q}} + \frac{1}{2} \sum_{\mathbf{K}, \mathbf{k}} \left(\delta U_\lambda(\mathbf{k}, \mathbf{q} - \mathbf{K}/2) a_{\mathbf{K}/2+\mathbf{k}}^\dagger a_{\mathbf{K}/2-\mathbf{k}}^\dagger a_{\mathbf{K}-\mathbf{q}} a_{\mathbf{q}} \right. \right. \\ &\quad \left. \left. + \delta U_\lambda^\dagger(\mathbf{q} - \mathbf{K}/2, \mathbf{k}) a_{\mathbf{q}}^\dagger a_{\mathbf{K}-\mathbf{q}}^\dagger a_{\mathbf{K}/2-\mathbf{k}} a_{\mathbf{K}/2+\mathbf{k}} \right) \right. \\ &\quad \left. + \frac{1}{4} \sum_{\mathbf{K}, \mathbf{k}, \mathbf{k}'} \delta U_\lambda(\mathbf{k}, \mathbf{q} - \mathbf{K}/2) \delta U_\lambda^\dagger(\mathbf{q} - \mathbf{K}/2, \mathbf{k}') a_{\mathbf{K}/2+\mathbf{k}}^\dagger a_{\mathbf{K}/2-\mathbf{k}}^\dagger a_{\mathbf{K}/2-\mathbf{k}'} a_{\mathbf{K}/2+\mathbf{k}'} \right] | \Psi_\lambda^A \rangle \end{aligned}$$

- Take continuum limit (suppressing spin and isospin labels): $\sum_{\mathbf{k}} \rightarrow \int d\mathbf{k}$

HF and LDA calculation

- Evaluating SRG-evolved operator with low RG resolution wave functions $\langle \Psi_\lambda^A | \hat{U}_\lambda \hat{n}^{hi}(\mathbf{q}) \hat{U}_\lambda^\dagger | \Psi_\lambda^A \rangle$

$$\begin{aligned} &\approx \langle \Psi_\lambda^A | \left[a_{\mathbf{q}}^\dagger a_{\mathbf{q}} + \frac{1}{2} \sum_{\mathbf{K}, \mathbf{k}} \left(\delta U_\lambda(\mathbf{k}, \mathbf{q} - \mathbf{K}/2) a_{\mathbf{K}/2+\mathbf{k}}^\dagger a_{\mathbf{K}/2-\mathbf{k}}^\dagger a_{\mathbf{K}-\mathbf{q}} a_{\mathbf{q}} \right. \right. \\ &\quad \left. \left. + \delta U_\lambda^\dagger(\mathbf{q} - \mathbf{K}/2, \mathbf{k}) a_{\mathbf{q}}^\dagger a_{\mathbf{K}-\mathbf{q}}^\dagger a_{\mathbf{K}/2-\mathbf{k}} a_{\mathbf{K}/2+\mathbf{k}} \right) \right. \\ &\quad \left. + \frac{1}{4} \sum_{\mathbf{K}, \mathbf{k}, \mathbf{k}'} \delta U_\lambda(\mathbf{k}, \mathbf{q} - \mathbf{K}/2) \delta U_\lambda^\dagger(\mathbf{q} - \mathbf{K}/2, \mathbf{k}') a_{\mathbf{K}/2+\mathbf{k}}^\dagger a_{\mathbf{K}/2-\mathbf{k}}^\dagger a_{\mathbf{K}/2-\mathbf{k}'} a_{\mathbf{K}/2+\mathbf{k}'} \right] | \Psi_\lambda^A \rangle \end{aligned}$$

- Take continuum limit (suppressing spin and isospin labels): $\sum_{\mathbf{k}} \rightarrow \int d\mathbf{k}$
- Evaluate matrix elements assuming $|\Psi_\lambda^A\rangle$ is occupied up to momentum k_F averaging over local Fermi momentum $k_F^\tau(R) = (3\pi^2 \rho^\tau(R))^{1/3}$

$$\langle \Psi_\lambda^A | a_{\frac{\mathbf{K}}{2}+\mathbf{k}}^\dagger a_{\frac{\mathbf{K}}{2}-\mathbf{k}}^\dagger a_{\frac{\mathbf{K}}{2}-\mathbf{k}'} a_{\frac{\mathbf{K}}{2}+\mathbf{k}'} | \Psi_\lambda^A \rangle \approx \int d\mathbf{R} \delta(\mathbf{k}' - \mathbf{k}) \theta(k_F^\tau(R) - |\mathbf{K}/2 + \mathbf{k}|) \theta(k_F^{\tau'}(R) - |\mathbf{K}/2 - \mathbf{k}|)$$

HF and LDA calculation

- Angle-average to evaluate angular dependence of $\mathbf{q} \cdot \mathbf{k}$, $\mathbf{q} \cdot \mathbf{K}$, and $\mathbf{K} \cdot \mathbf{k}$ (defines angles x , y , and z)

E.g.,
$$\int_{-1}^1 \frac{dz}{2} \theta(k_F^\tau - |\mathbf{K}/2 + \mathbf{k}|) \theta(k_F^{\tau'} - |\mathbf{K}/2 - \mathbf{k}|) = \begin{cases} 1 & \text{if } k < k_F^{\min} - \frac{K}{2} \\ \frac{(k_F^{\min})^2 - (k - K/2)^2}{2kK} & \text{if } k < k_F^{\min} + \frac{K}{2} \text{ and} \\ & k_F^{\min} - \frac{K}{2} < k < k_F^{\max} - \frac{K}{2} \\ \frac{(k_F^{\text{avg}})^2 - k^2 - K^2/4}{kK} & \text{if } k_F^{\max} - \frac{K}{2} < k \text{ and} \\ & k < \sqrt{(k_F^{\text{avg}})^2 - \frac{K^2}{4}} \\ 0 & \text{otherwise} \end{cases}$$
 where $\left| \frac{\mathbf{K}}{2} + \mathbf{k} \right| = \sqrt{\frac{K^2}{4} + k^2 + Kkz}$

HF and LDA calculation

- Angle-average to evaluate angular dependence of $\mathbf{q} \cdot \mathbf{k}$, $\mathbf{q} \cdot \mathbf{K}$, and $\mathbf{K} \cdot \mathbf{k}$ (defines angles x , y , and z)

E.g.,
$$\int_{-1}^1 \frac{dz}{2} \theta(k_F^\tau - |\mathbf{K}/2 + \mathbf{k}|) \theta(k_F^{\tau'} - |\mathbf{K}/2 - \mathbf{k}|) = \begin{cases} 1 & \text{if } k < k_F^{\min} - \frac{K}{2} \\ \frac{(k_F^{\min})^2 - (k - K/2)^2}{2kK} & \text{if } k < k_F^{\min} + \frac{K}{2} \text{ and} \\ & k_F^{\min} - \frac{K}{2} < k < k_F^{\max} - \frac{K}{2} \\ \frac{(k_F^{\text{avg}})^2 - k^2 - K^2/4}{kK} & \text{if } k_F^{\max} - \frac{K}{2} < k \text{ and} \\ & k < \sqrt{(k_F^{\text{avg}})^2 - \frac{K^2}{4}} \\ 0 & \text{otherwise} \end{cases}$$

where $\left| \frac{\mathbf{K}}{2} + \mathbf{k} \right| = \sqrt{\frac{\mathbf{K}^2}{4} + k^2 + Kkz}$

- Finally write in terms of partial waves using

$$|\mathbf{k}_1 \sigma_1 \tau_1 \mathbf{k}_2 \sigma_2 \tau_2\rangle = \frac{1}{\sqrt{2}} \sum_{S,M_S} \sum_{L,M_L} \sum_{J,M_J} \sum_{T,M_T} \langle \sigma_1 \sigma_2 | S M_S \rangle \langle \tau_1 \tau_2 | T M_T \rangle \sqrt{\frac{2}{\pi}} Y_{L,M_L}^*(\hat{k}) \langle L M_L S M_S | J M_J \rangle [1 - (-1)^{L+S+T}] |\mathbf{K} k(LS) J M_J T M_T\rangle$$

where $\mathbf{k} \equiv \frac{1}{2}(\mathbf{k}_1 - \mathbf{k}_2)$ and $\mathbf{K} \equiv \mathbf{k}_1 + \mathbf{k}_2$

HF and LDA calculation

- Final formula for single-nucleon momentum distribution (where τ specifies proton or neutron) given by:

$$\begin{aligned} n_\lambda^\tau(q) = & \int d^3R \left\{ 2\theta(k_{\text{F}}^\tau - q) + 32 \sum'_{L,S,T} \sum_J (2J+1) \frac{2}{\pi} \int_0^\infty dk k^2 (k(LS)JT | \delta U | k(LS)JT) \sum_{\tau'} |\langle \tau \tau' | T \tau + \tau' \rangle|^2 \theta(k_{\text{F}}^\tau - q) \right. \\ & \times \int_{-1}^1 \frac{dx}{2} \theta(k_{\text{F}}^{\tau'} - |\mathbf{q} - 2\mathbf{k}|) + 2 \sum'_{L,L',S,T} \sum_J (2J+1) \left(\frac{2}{\pi} \right)^2 \int_0^\infty dk k^2 \int_0^\infty dK K^2 \int_{-1}^1 \frac{dy}{2} \\ & \times \int_{-1}^1 \frac{dz}{2} (k(LS)JT | \delta U | |\mathbf{q} - \mathbf{K}/2| (L'S)JT) (|\mathbf{q} - \mathbf{K}/2| (L'S)JT | \delta U^\dagger | k(LS)JT) \\ & \left. \times \sum_{\tau'} |\langle \tau \tau' | T \tau + \tau' \rangle|^2 \theta(k_{\text{F}}^\tau - |\mathbf{K}/2 + \mathbf{k}|) \theta(k_{\text{F}}^{\tau'} - |\mathbf{K}/2 - \mathbf{k}|) \right\}, \end{aligned}$$

Proton momentum distributions

- Low RG resolution calculations reproduce momentum distributions of AV18 VMC calculations¹ (high RG resolution)

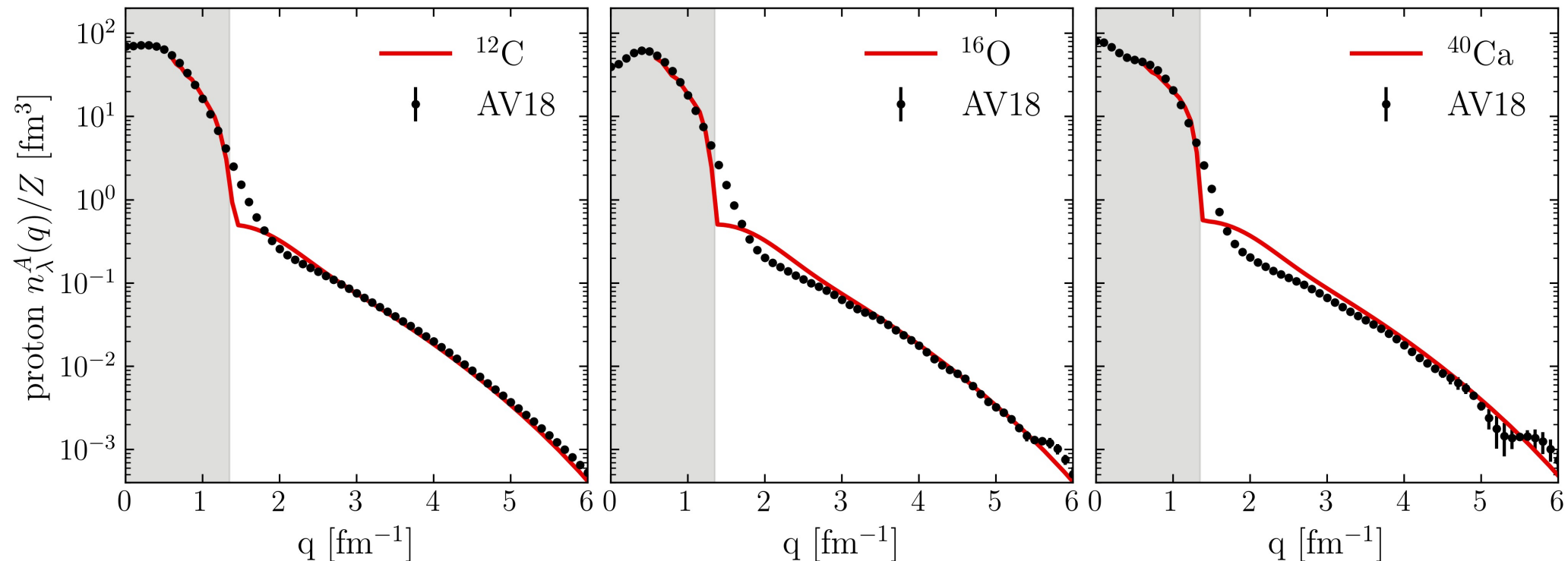


Fig. 6: Proton momentum distributions for ^{12}C , ^{16}O , and ^{40}Ca under HF+LDA with AV18, $\lambda = 1.35$ fm⁻¹, and densities from Skyrme EDF SLy4 using the HFBRAD code².

Proton momentum distributions

- Low RG resolution calculations reproduce momentum distributions of AV18 VMC calculations¹ (high RG resolution)

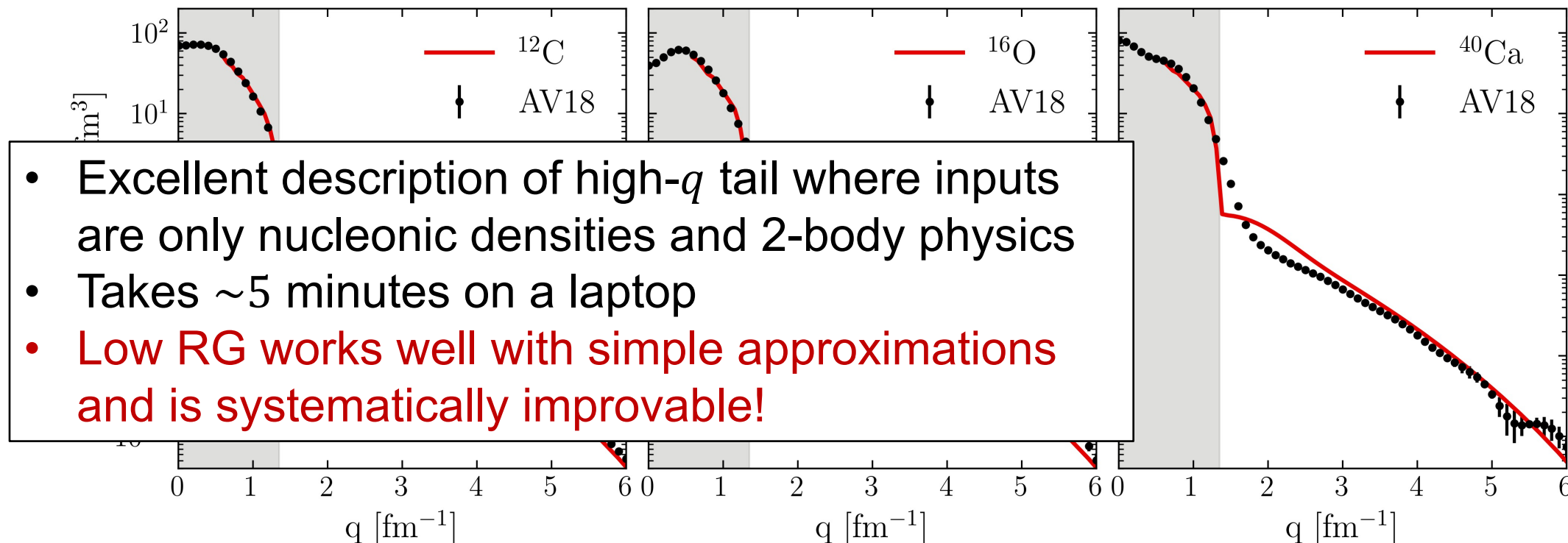
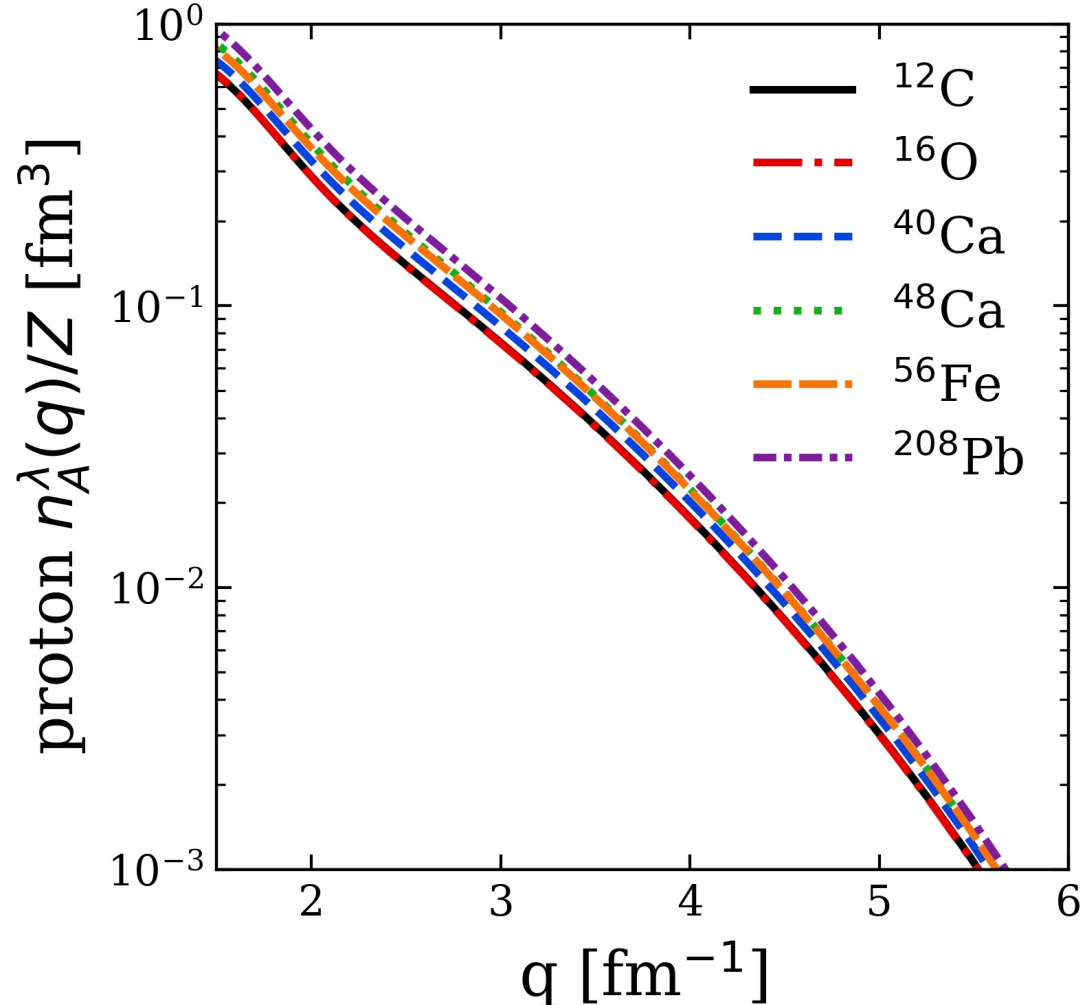


Fig. 6: Proton momentum distributions for ^{12}C , ^{16}O , and ^{40}Ca under HF+LDA with AV18, $\lambda = 1.35 \text{ fm}^{-1}$, and densities from Skyrme EDF SLy4 using the HFBRAD code².

Proton momentum distributions



- **Universality:** High- q dependence from universal function $\approx |F_\lambda^{hi}(q)|^2$ fixed by 2-body and insensitive to nucleus

Fig. 7: Proton momentum distributions under HF+LDA with AV18 and $\lambda = 1.35 \text{ fm}^{-1}$, showing several nuclei.

Proton momentum distributions

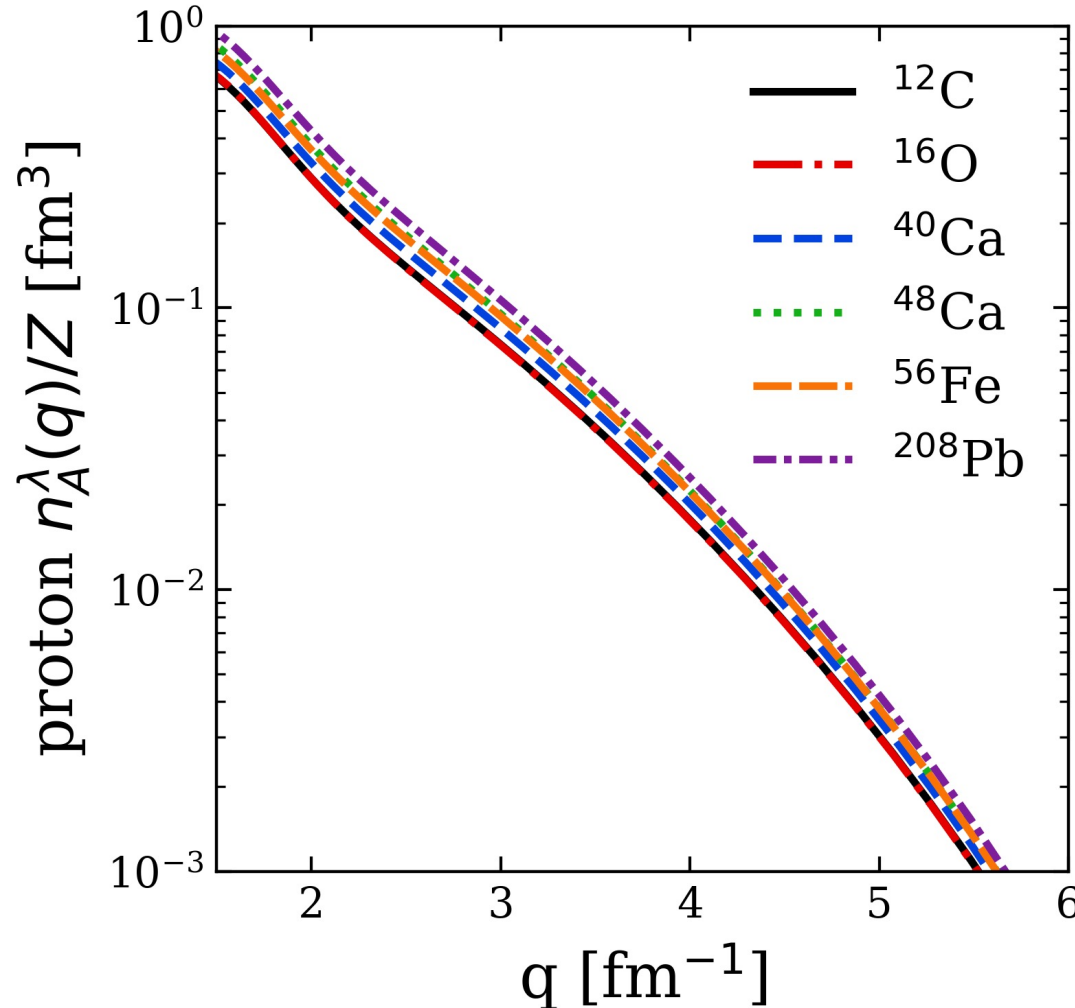
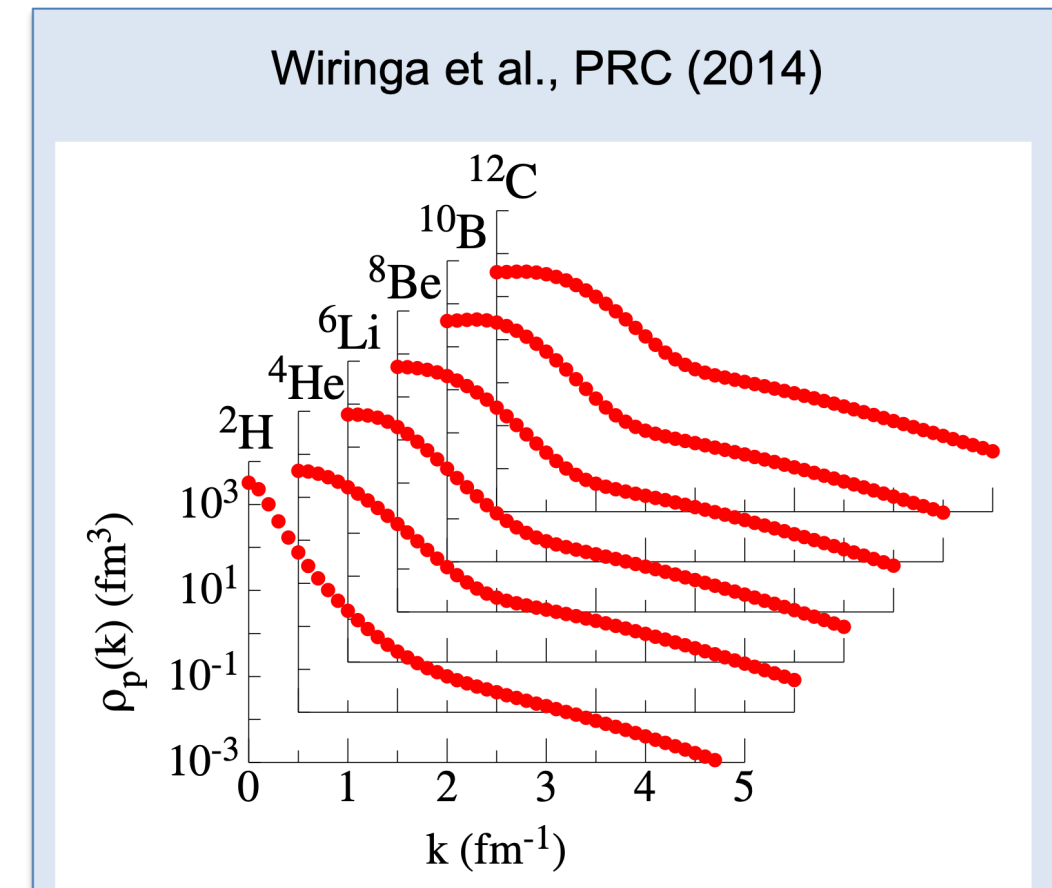
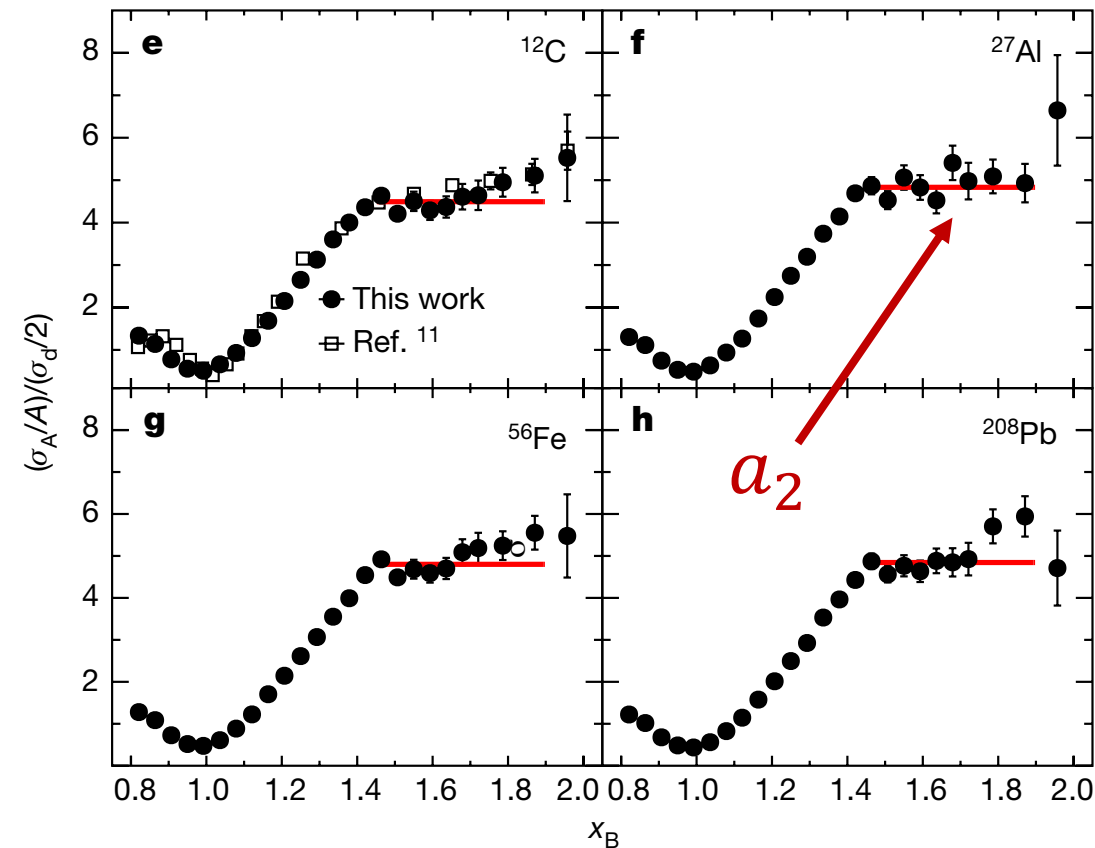


Fig. 7: Proton momentum distributions under HF+LDA with AV18 and $\lambda = 1.35$ fm $^{-1}$, showing several nuclei.



Consistent with universal high- q tails from VMC calculations of R. B. Wiringa et al., Phys. Rev. C **89**, 024305 (2014)

SRC scaling factors



- SRC scaling factors a_2 defined by plateau in cross section ratio $\frac{2\sigma_A}{A\sigma_d}$ at $1.45 \leq x \leq 1.9$
- Closely related to the ratio of bound-nucleon probability distributions in the limits of vanishing relative distance (infinitely high relative momentum)
- Extract a_2 from momentum distributions

$$a_2 = \lim_{q \rightarrow \infty} \frac{P^A(q)}{P^d(q)} \approx \frac{\int_{\Delta q^{high}} dq P^A(q)}{\int_{\Delta q^{high}} dq P^d(q)}$$

where $P^A(q)$ is the single-nucleon probability distribution in nucleus A

Fig. 8: Ratio of per-nucleon electron scattering cross section of nucleus A to that of deuterium, where the red line indicates a constant fit. Figure from B. Schmookler et al. (CLAS), Nature **566**, 354 (2019).

SRC scaling factors

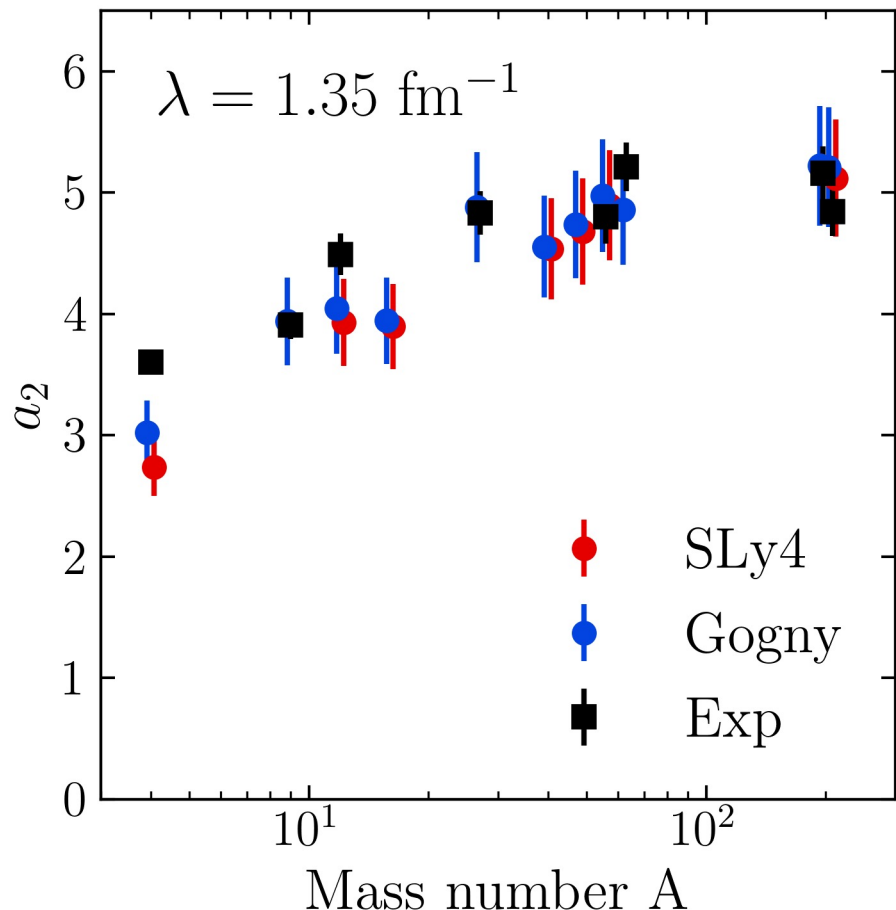


Fig. 9: a_2 scale factors using single-nucleon momentum distributions under HF+LDA (SLy4 in red¹, Gogny² in blue) with AV18 and $\lambda = 1.35 \text{ fm}^{-1}$ compared to experimental values³.

$$a_2 = \lim_{q \rightarrow \infty} \frac{P^A(q)}{P^d(q)} \approx \frac{\int_{\Delta q^{high}} dq P^A(q)}{\int_{\Delta q^{high}} dq P^d(q)}$$

- High momentum behavior is characterized by 2-body $|F_\lambda^{hi}(q)|^2$ which cancels leaving ratio of mean-field (low- k) physics
- Good agreement with a_2 values from experiment³ and LCA calculations⁴ using two different EDFs
- Error bars from varying Δq^{high}

SRC phenomenology

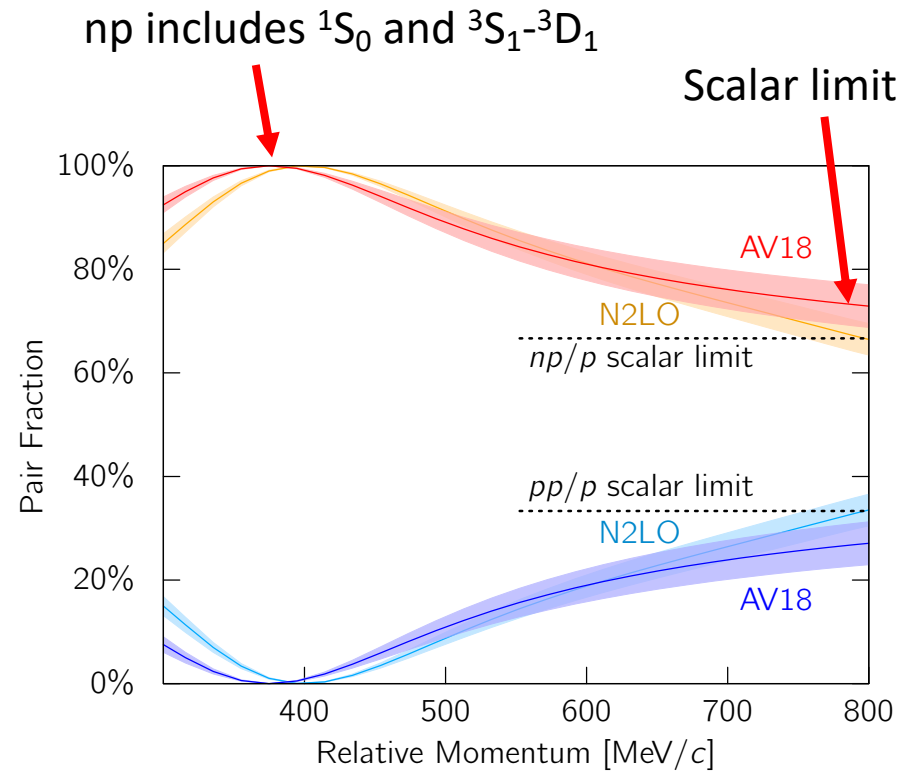
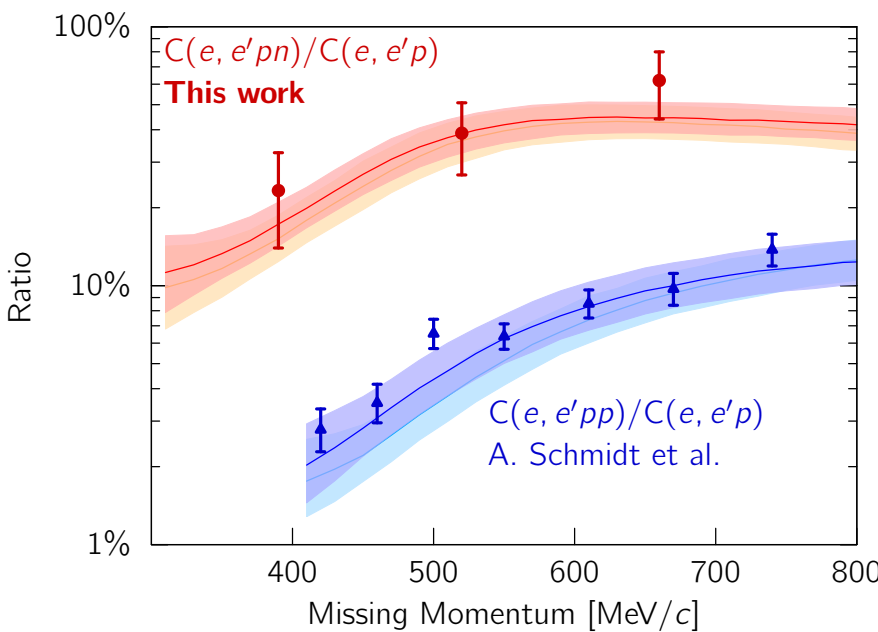


Fig. 10: (a) Ratio of two-nucleon to single-nucleon electron-scattering cross sections for carbon as a function of missing momentum. (b) Fraction of np to p and pp to p pairs versus the relative momentum. Figure from CLAS collaboration publication¹.

- At **high RG resolution**, the tensor force and the repulsive core of the NN interaction kicks nucleon pairs into SRCs
- np dominates because the tensor force requires spin triplet pairs, whereas pp are spin singlets
- **Do we describe this physics at low RG resolution?**

¹I. Korover et al. (CLAS), arXiv:2004.07304 (2014)

SRC phenomenology

- At **low RG resolution**, SRCs are suppressed in the wave function and shifted into the operator

$$\hat{n}^{lo}(\mathbf{q}) = \hat{U}_\lambda a_\mathbf{q}^\dagger a_\mathbf{q} \hat{U}_\lambda^\dagger = U_\lambda(\mathbf{k}, \mathbf{q}) U_\lambda^\dagger(\mathbf{q}, \mathbf{k}')$$

- Take ratio of 3S_1 and 1S_0 SRG transformations fixing low-momenta to $k_0 = 0.1 \text{ fm}^{-1}$
- This physics is established in the 2-body system – can apply to any nucleus!

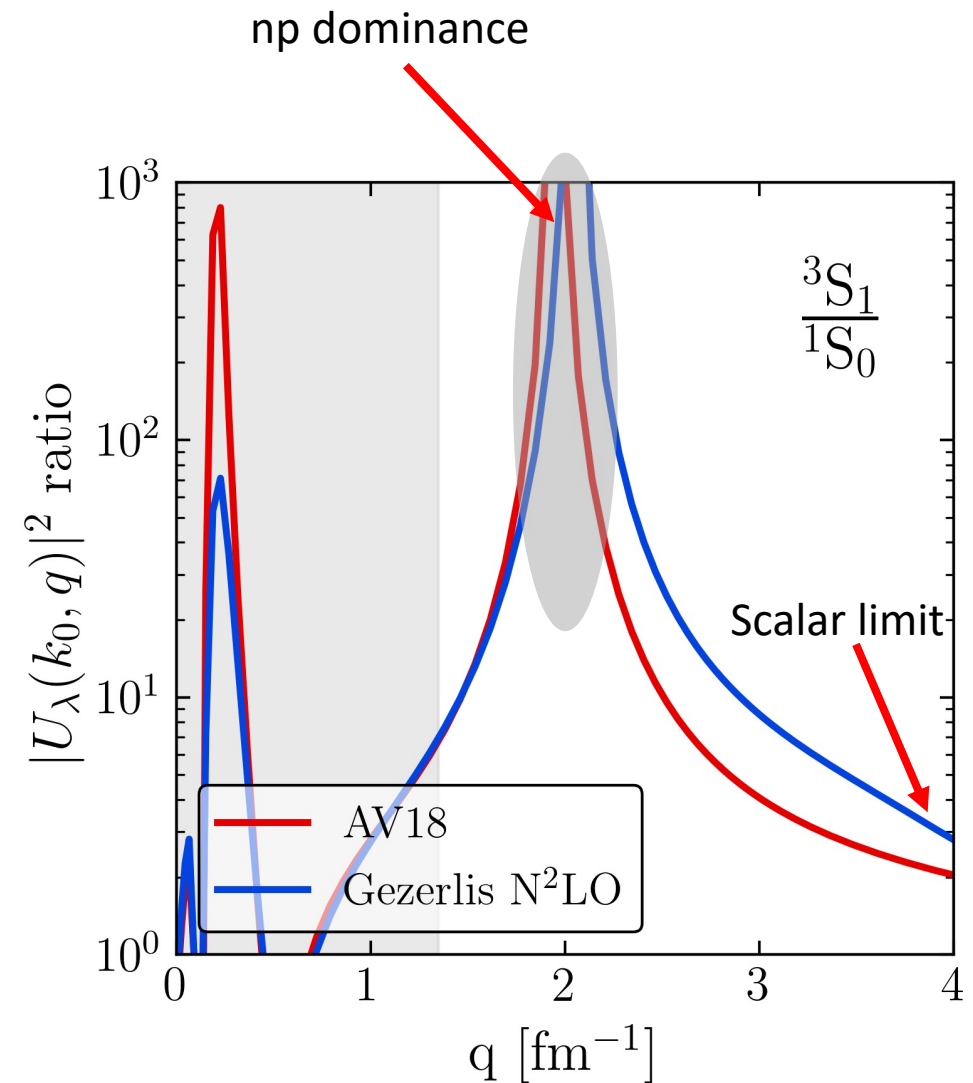
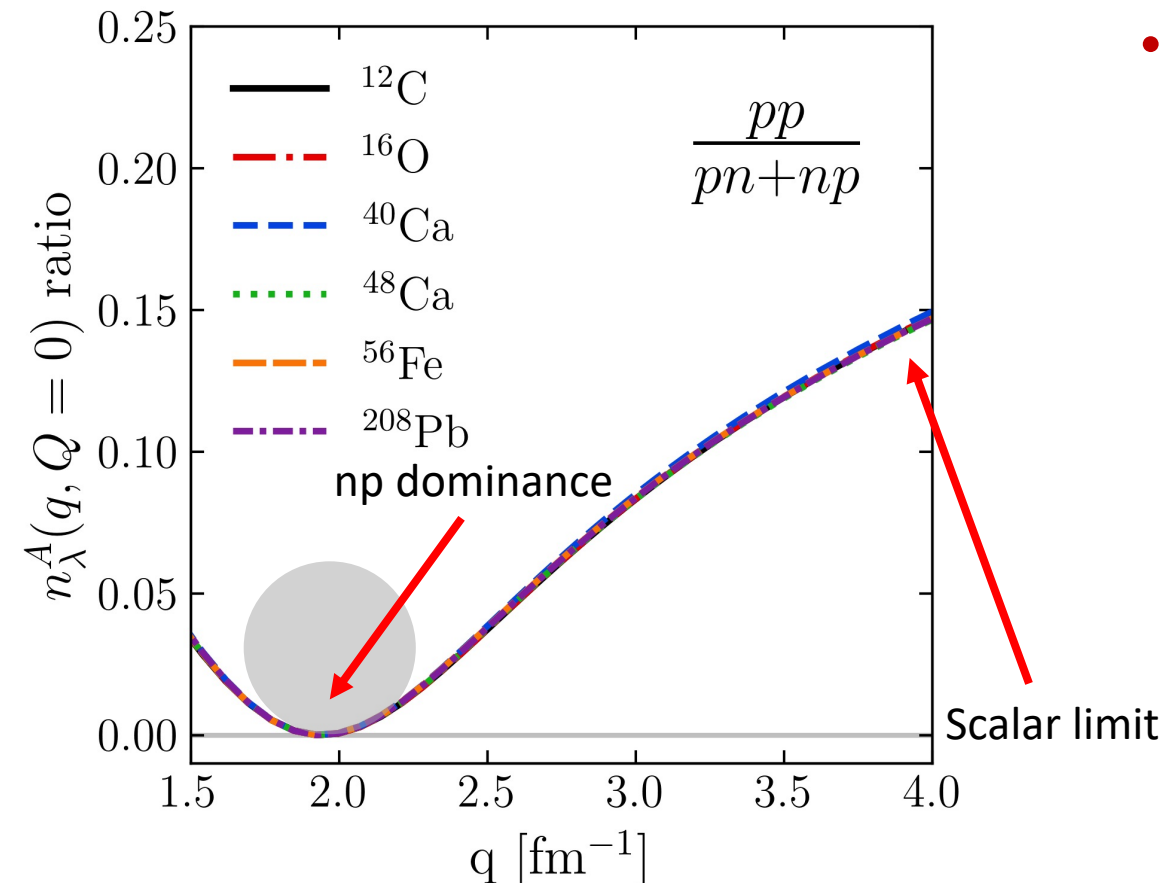


Fig. 11: 3S_1 to 1S_0 ratio of SRG-evolved momentum projection operators $a_q^\dagger a_q$ where $\lambda = 1.35 \text{ fm}^{-1}$.

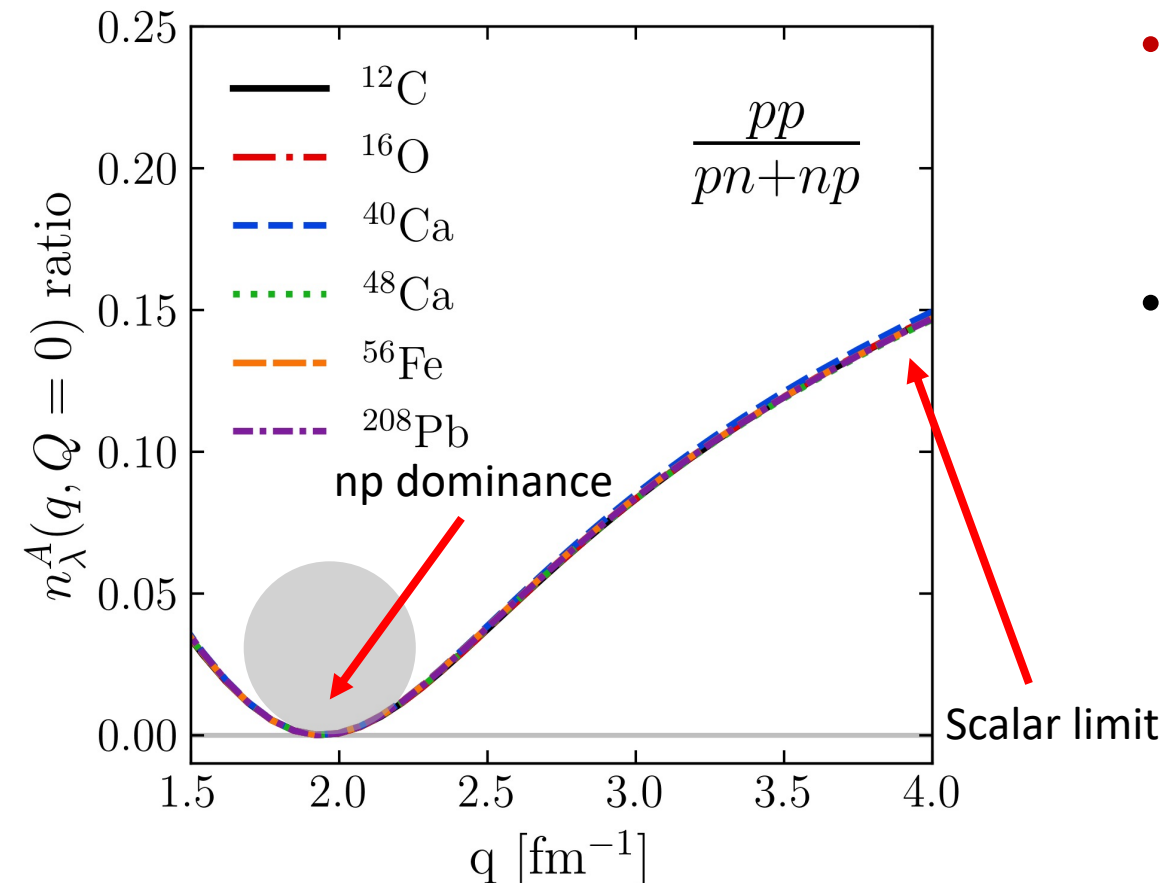
SRC phenomenology



- Low RG resolution picture reproduces the characteristics of cross section ratios using simple approximations

Fig. 12: pp/pn ratio of pair momentum distributions under HF+LDA with AV18 and $\lambda = 1.35$ fm $^{-1}$.

SRC phenomenology

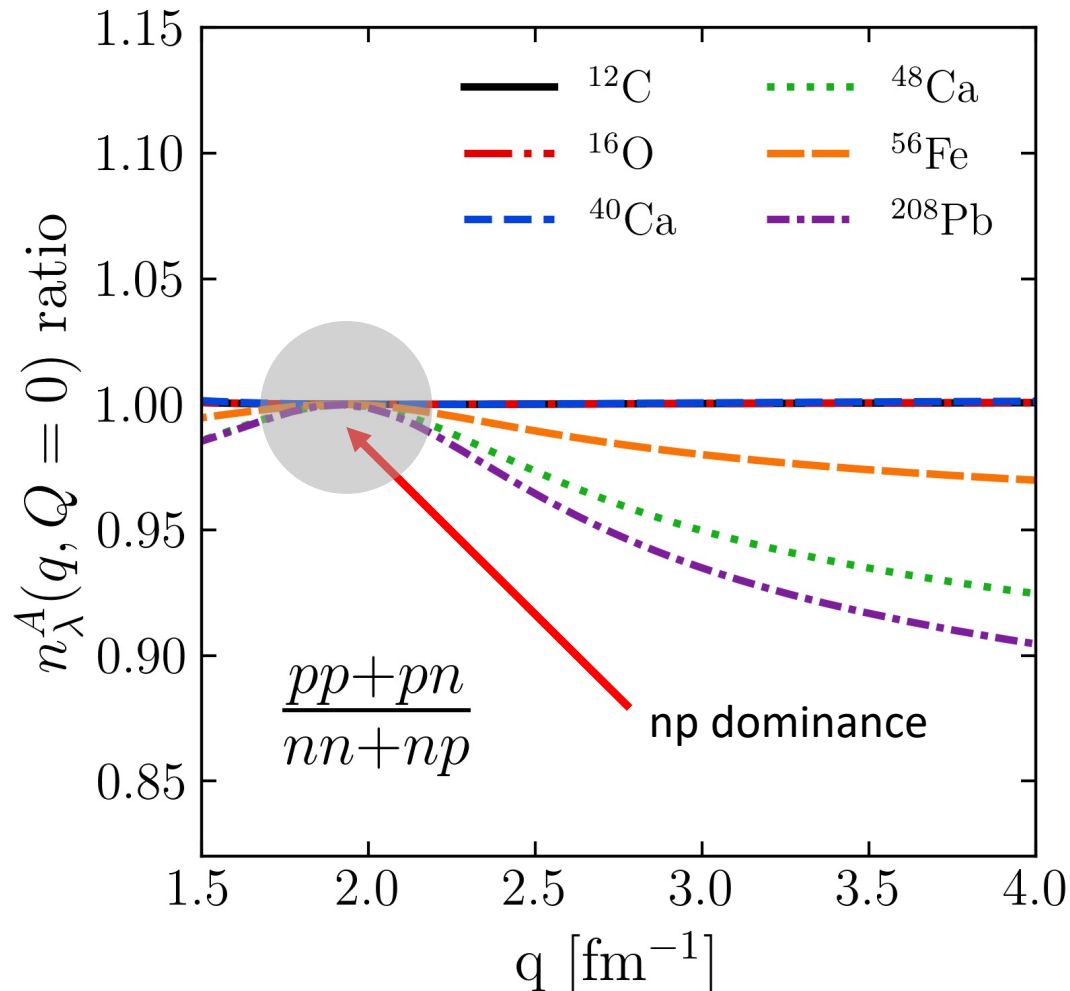


- Low RG resolution picture reproduces the characteristics of cross section ratios using simple approximations
- Weak nucleus dependence from factorization

$$\text{Ratio} \approx \frac{|F_{pp}^{hi}(\mathbf{q})|^2}{|F_{np}^{hi}(\mathbf{q})|^2} \times \frac{\left\langle \Psi_\lambda^A \left| \sum_{\mathbf{k}, \mathbf{k}'} \alpha_{\frac{\mathbf{Q}}{2} + \mathbf{k}}^\dagger \alpha_{\frac{\mathbf{Q}}{2} - \mathbf{k}}^\dagger \alpha_{\frac{\mathbf{Q}}{2} - \mathbf{k}'} \alpha_{\frac{\mathbf{Q}}{2} + \mathbf{k}'} \right| \Psi_\lambda^A \right\rangle}{\left\langle \Psi_\lambda^A \left| \sum_{\mathbf{k}, \mathbf{k}'} \alpha_{\frac{\mathbf{Q}}{2} + \mathbf{k}}^\dagger \alpha_{\frac{\mathbf{Q}}{2} - \mathbf{k}}^\dagger \alpha_{\frac{\mathbf{Q}}{2} - \mathbf{k}'} \alpha_{\frac{\mathbf{Q}}{2} + \mathbf{k}'} \right| \Psi_\lambda^A \right\rangle}$$

Fig. 12: pp/pn ratio of pair momentum distributions under HF+LDA with AV18 and $\lambda = 1.35$ fm^{-1} .

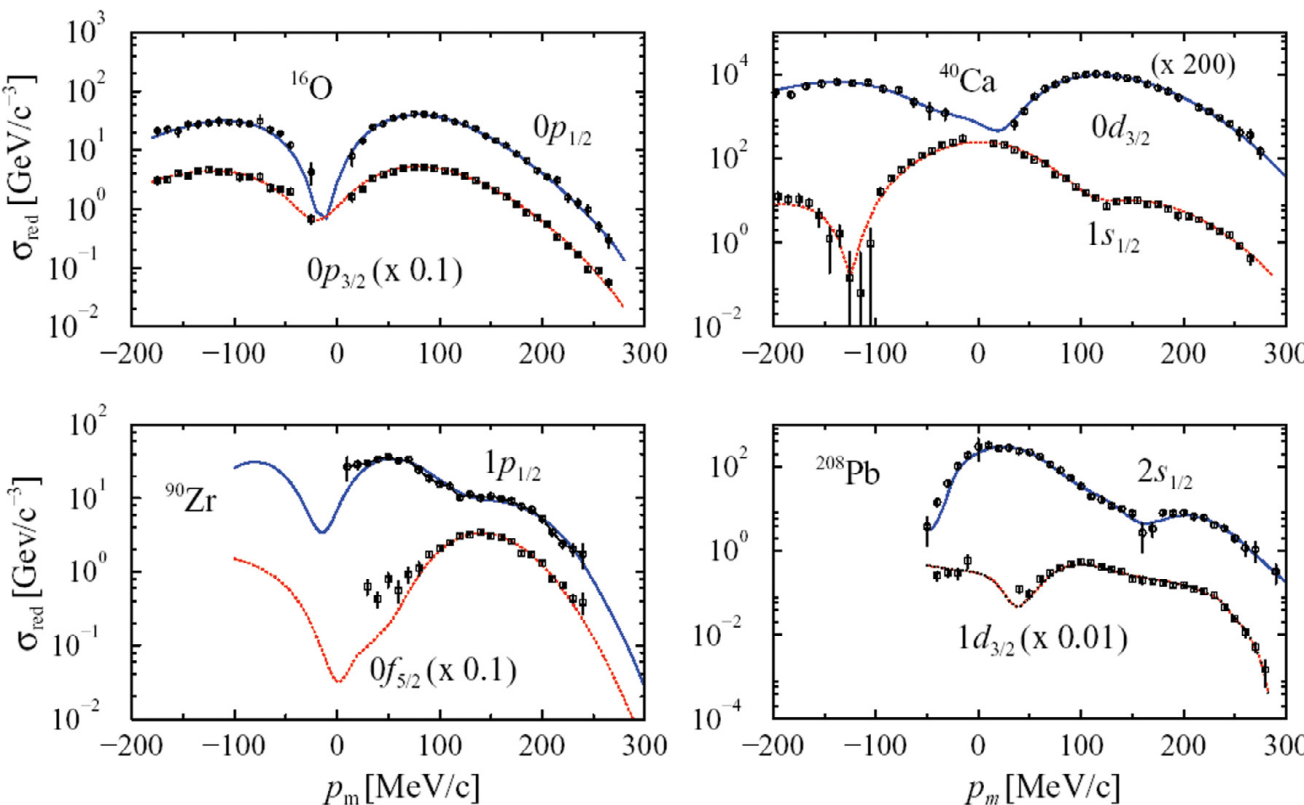
SRC phenomenology



- Ratio ~ 1 independent of N/Z in np dominant region
- Ratio < 1 for nuclei where $N > Z$ and outside np dominant region

Fig. 13: $(\text{pp}+\text{pn})/(\text{nn}+\text{np})$ ratio of pair momentum distributions under HF+LDA with AV18 and $\lambda = 1.35 \text{ fm}^{-1}$.

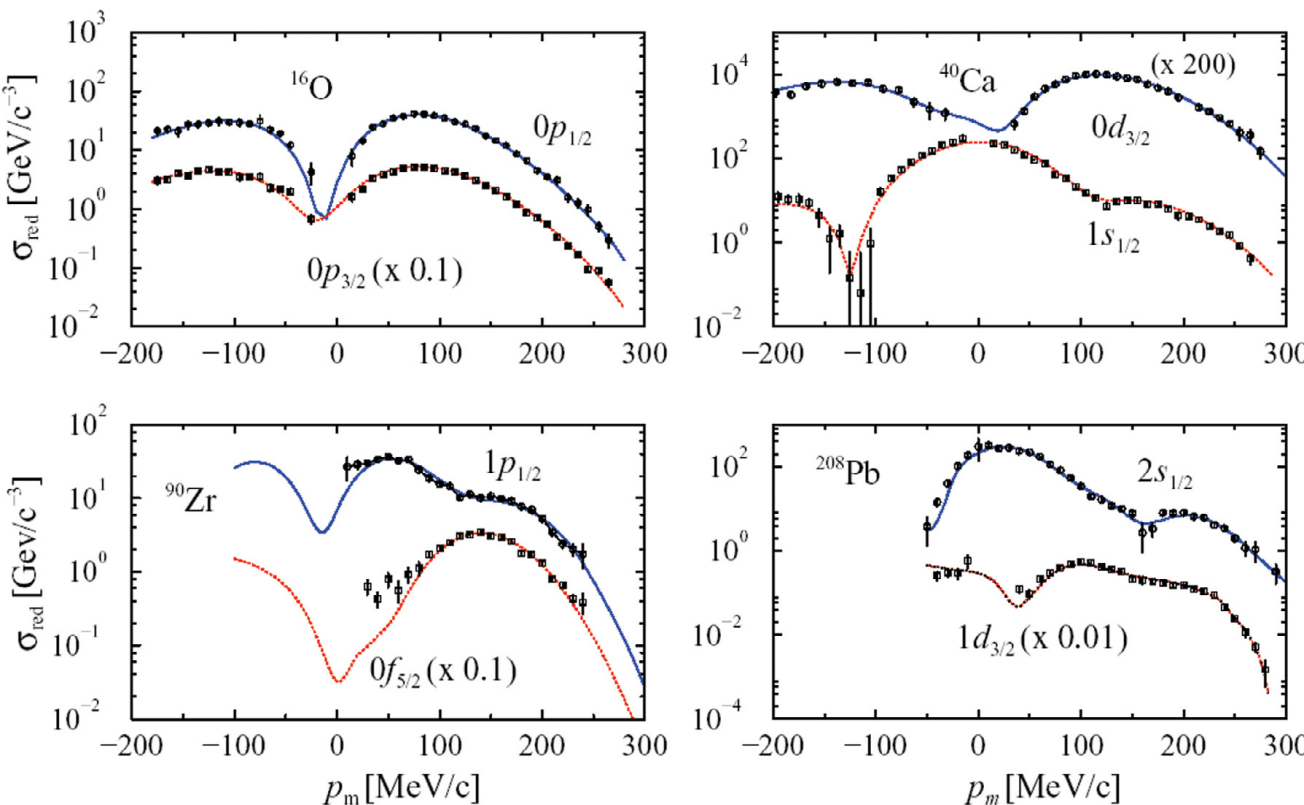
Other exclusive knockout reactions



- Apply similar low RG analysis to exclusive knockout reactions in $(e,e'p)$ scattering
- Nucleon knocked out from specific shell model state of target nucleus A

Fig. 14: Momentum profiles as function of missing momentum for valence holes in nuclei. Data (black points) from NIKHEF experiments. Figure from T. Aumann et al., Prog. Part. Nucl. Phys. **118**, 103847 (2021).

Other exclusive knockout reactions



- Apply similar low RG analysis to exclusive knockout reactions in $(e,e'p)$ scattering
- Nucleon knocked out from specific shell model state of target nucleus A
- Momentum dependence of $(e,e'p)$ exclusive cross section is dominated by the single-particle (sp) wave function
- **Spectroscopic factor needed to reduce the theoretical cross section to match experiment**

Fig. 14: Momentum profiles as function of missing momentum for valence holes in nuclei. Data (black points) from NIKHEF experiments. Figure from T. Aumann et al., Prog. Part. Nucl. Phys. **118**, 103847 (2021).

Other exclusive knockout reactions

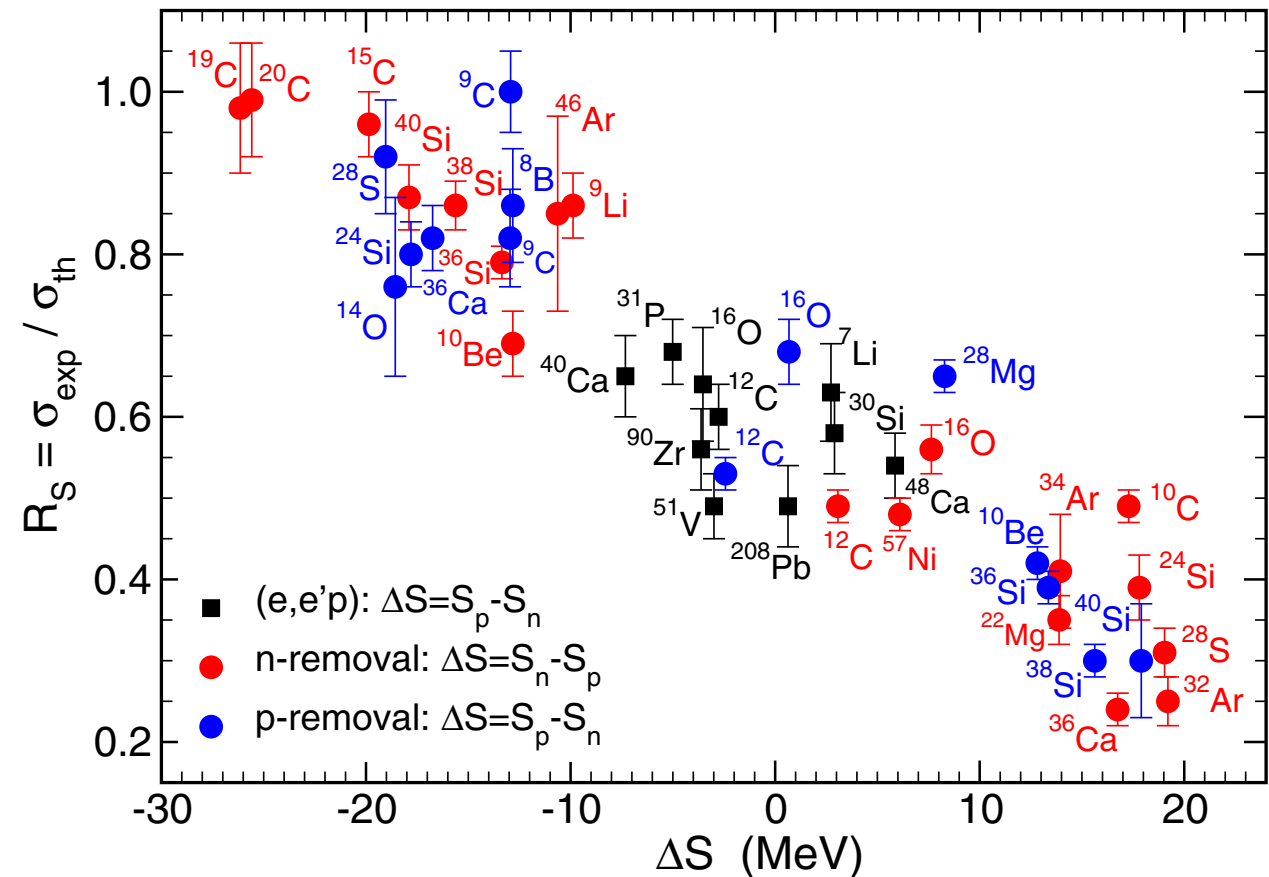


Fig. 15: R as a function of ΔS . Red (blue) points correspond to neutron-removal (proton-removal) cases. Solid black squares correspond to electron-induced proton knockout data. Figure from J. A. Tostevin and A. Gade, Phys. Rev. C **90**, 057602 (2014).

- Systematic trend for discrepancy in exp/theory as a function of ΔS
- RG analysis can help understand the cause of $R = \frac{\sigma_{\text{exp}}}{\sigma_{\text{theory}}} < 1$
- Mismatch of scale between one-body (**high RG**) operator and shell model structure (**low RG**) gives $\sigma_{\text{theory}} > \sigma_{\text{exp}}$

Other exclusive knockout reactions

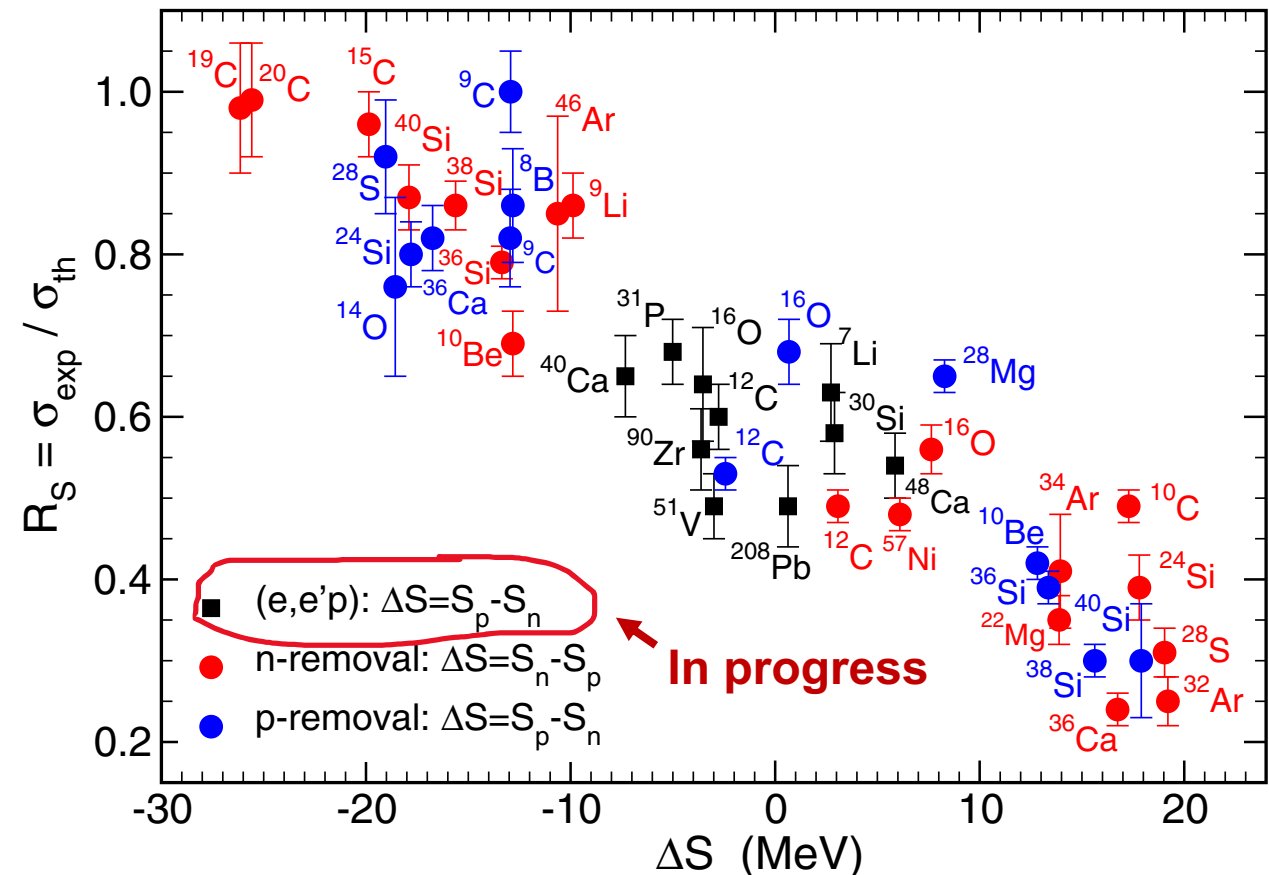


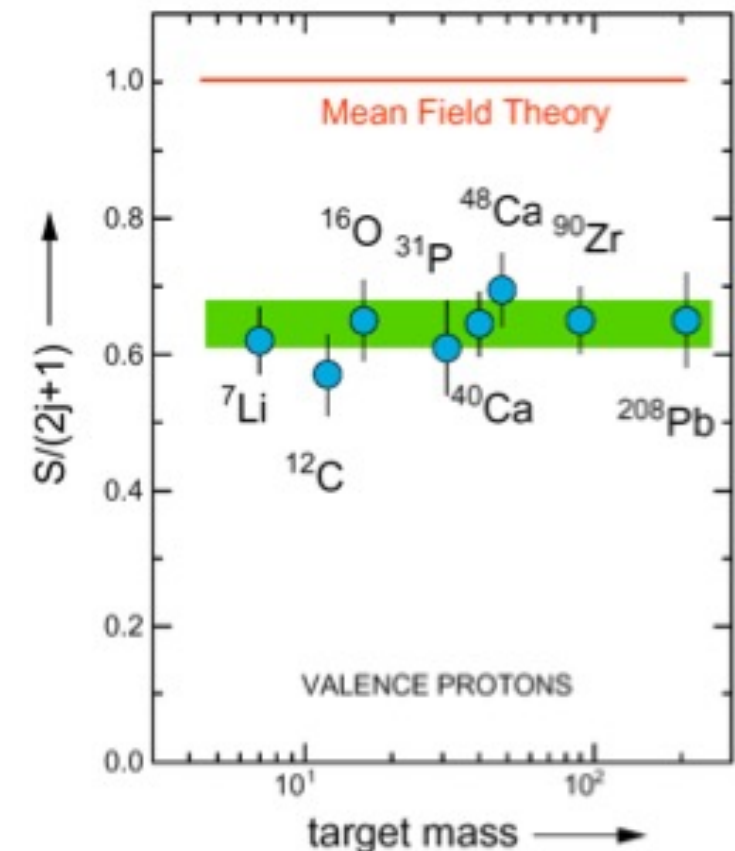
Fig. 15: R as a function of ΔS . Red (blue) points correspond to neutron-removal (proton-removal) cases. Solid black squares correspond to electron-induced proton knockout data. Figure from J. A. Tostevin and A. Gade, Phys. Rev. C **90**, 057602 (2014).

- Systematic trend for discrepancy in exp/theory as a function of ΔS
- RG analysis can help understand the cause of $R = \frac{\sigma_{exp}}{\sigma_{theory}} < 1$
- Mismatch of scale between one-body (**high RG**) operator and shell model structure (**low RG**) gives $\sigma_{theory} > \sigma_{exp}$
- Currently working on SRG-evolving spectroscopic factors for $(e, e'p)$ reactions
- Note, spectroscopic factors are scale/scheme dependent

Spectroscopic factors

- Spectroscopic factor for sp state α defined in terms of removal amplitude

$$S = \int d\mathbf{p} |\langle \Psi_{\alpha}^{A-1} | a_{\mathbf{p}} | \Psi_0^A \rangle|^2$$

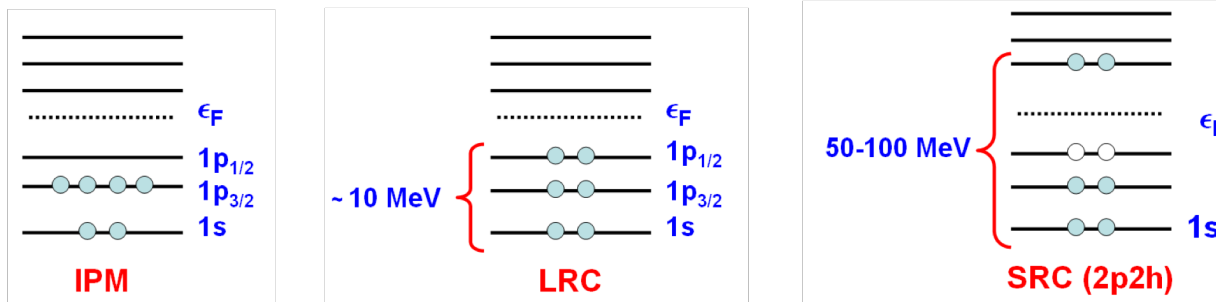


Spectroscopic factors

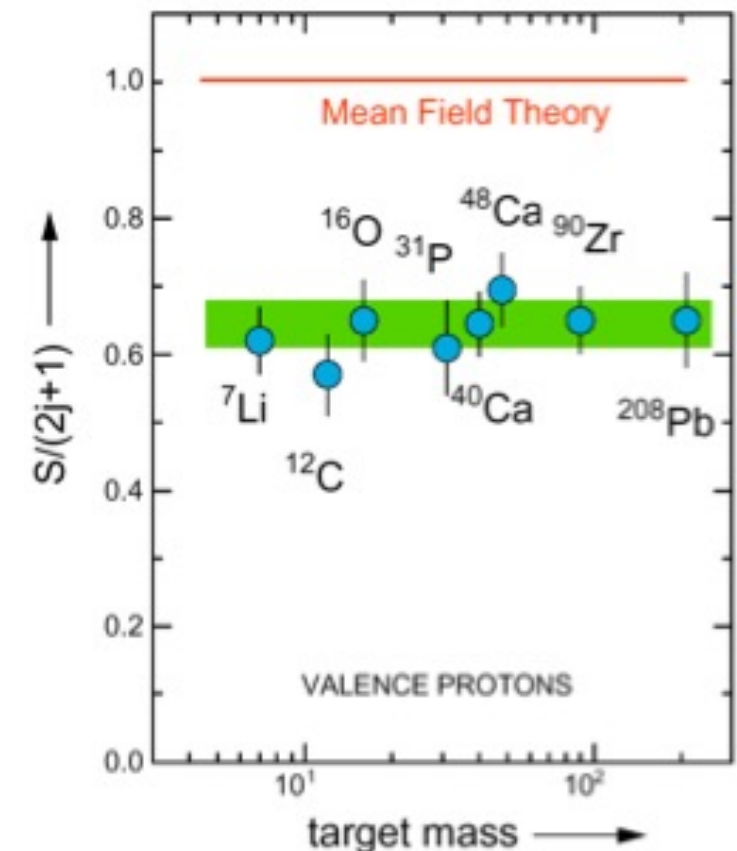
- Spectroscopic factor for sp state α defined in terms of removal amplitude

$$S = \int d\mathbf{p} |\langle \Psi_{\alpha}^{A-1} | a_{\mathbf{p}} | \Psi_0^A \rangle|^2$$

- sp strength is reduced relative to the independent-particle model (IPM) by correlations: **Long-range correlations (LRC)** and **SRC**



Long-range vs. short-range correlations



Spectroscopic factors

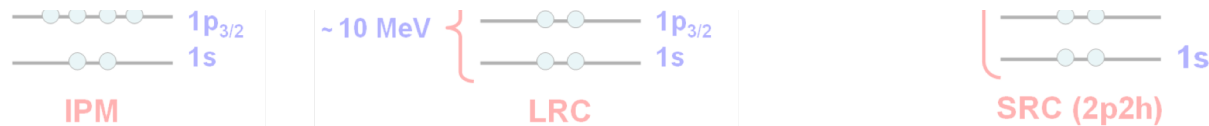
- Spectroscopic factor for sp state α defined in terms of removal amplitude

$$S = \int d\mathbf{p} |\langle \Psi_{\alpha}^{A-1} | a_{\mathbf{p}} | \Psi_0^A \rangle|^2$$

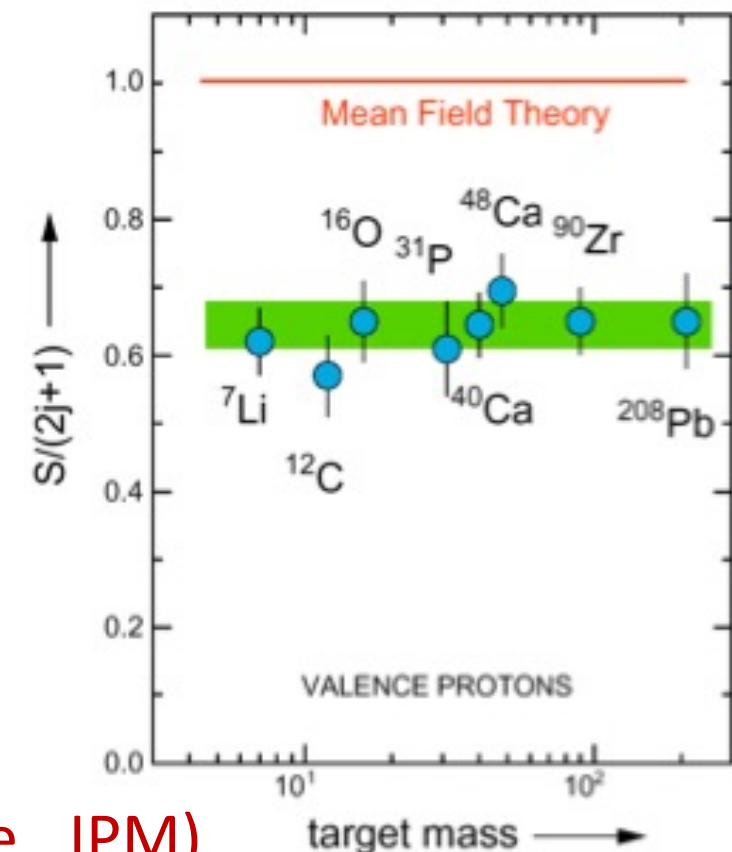
- sp strength is reduced relative to the independent-particle model (IPM) by correlations: **Long-range correlations (LRC)** and **SRC**



Idea: SRG evolve and analyze using simple approximations (i.e., IPM)



Long-range vs. short-range correlations



Summary

- At low renormalization group (RG) resolution, simple approximations to SRC physics work and are systematically improvable
- Results suggest that we can analyze high-energy nuclear reactions using low RG resolution structure (e.g., shell model) and consistently evolved operators
 - Matching resolution scale between structure and reactions is crucial!

Summary

- At low renormalization group (RG) resolution, simple approximations to SRC physics work and are systematically improvable
- Results suggest that we can analyze high-energy nuclear reactions using low RG resolution structure (e.g., shell model) and consistently evolved operators
 - Matching resolution scale between structure and reactions is crucial!
- **Outlook:**
 - Extend to $(e, e' p)$ and other knockout reactions and test scale/scheme dependence of extracted properties
 - Benchmark calculations with other ab initio methods
 - Investigate impact of various corrections: 3-body terms, final state interactions, etc.
 - Implement uncertainty quantification in low RG resolution calculations

Extras

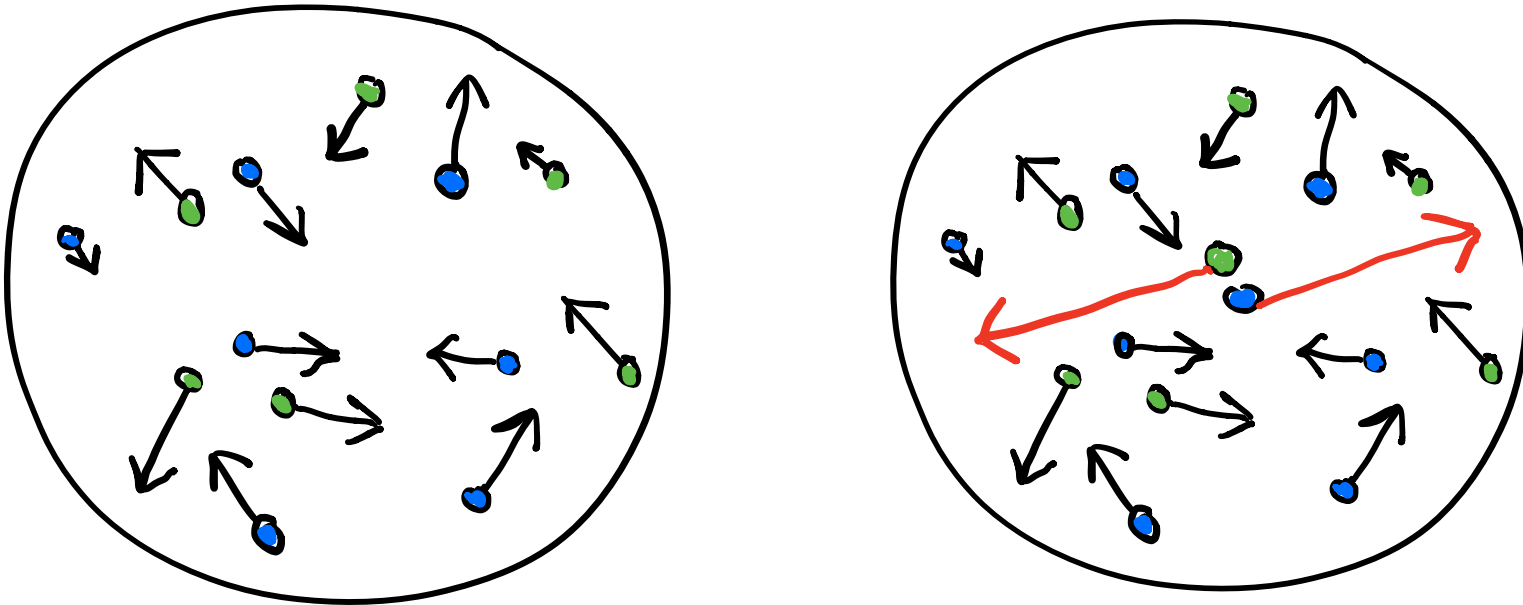
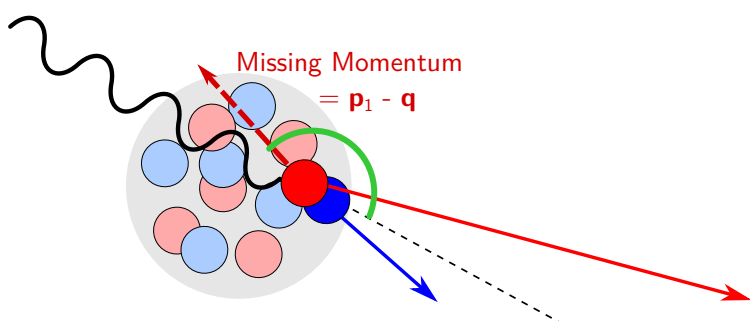
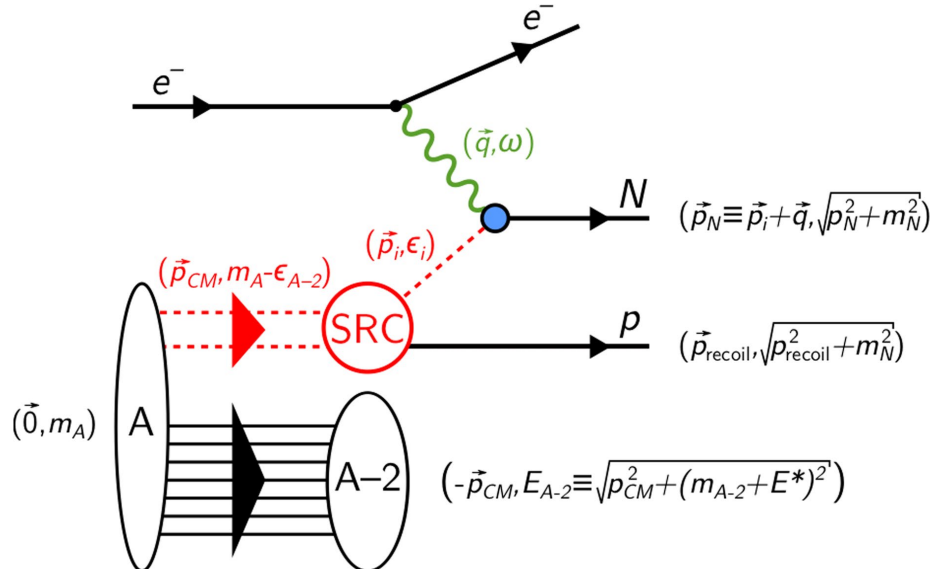


Fig. 16: Cartoon snapshots of a nucleus at (left) low-RG and (right) high-RG resolutions. The back-to-back nucleons at high-RG resolution are an SRC pair with small center-of-mass momentum.

Extras



- Kinematics chosen such that two-nucleon knock-out dominates
- Break up the pair, detect both nucleons, and reconstruct initial state
- Kinematics minimize final state interactions and meson exchange currents

Extras

Universality: Low-energy physics of different interactions becomes the same at low RG resolution

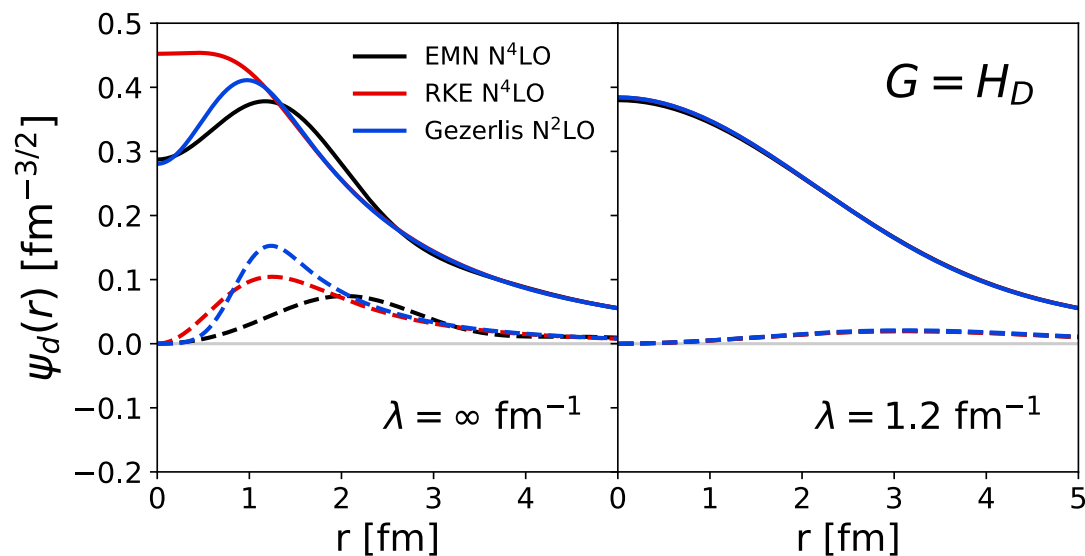


Fig. 17: Initial and SRG-evolved deuteron wave functions in coordinate space for several chiral interactions.

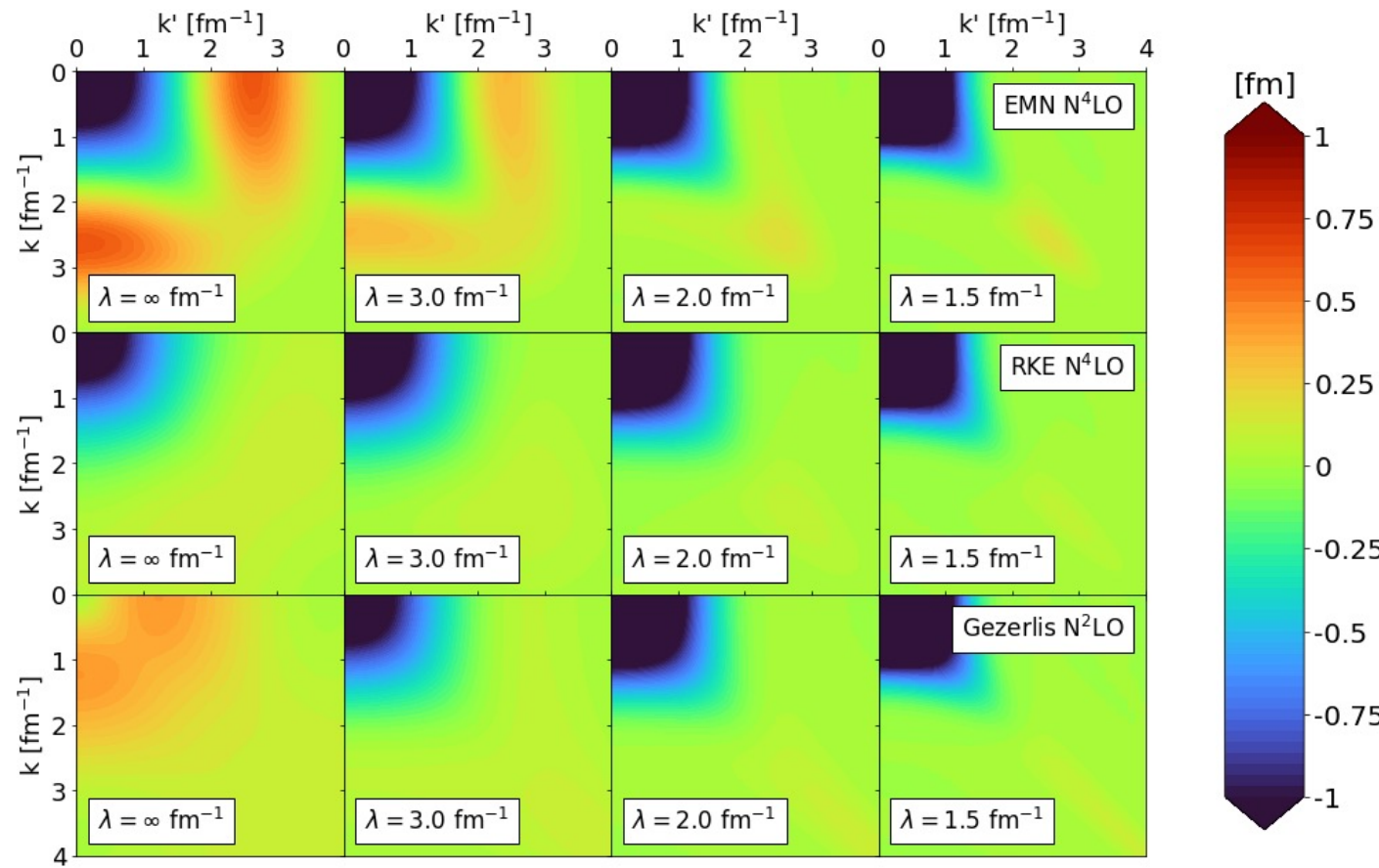


Fig. 18: SRG evolution for several chiral interactions in the $^3\text{S}_1 - ^3\text{S}_1$ channel.

Extras

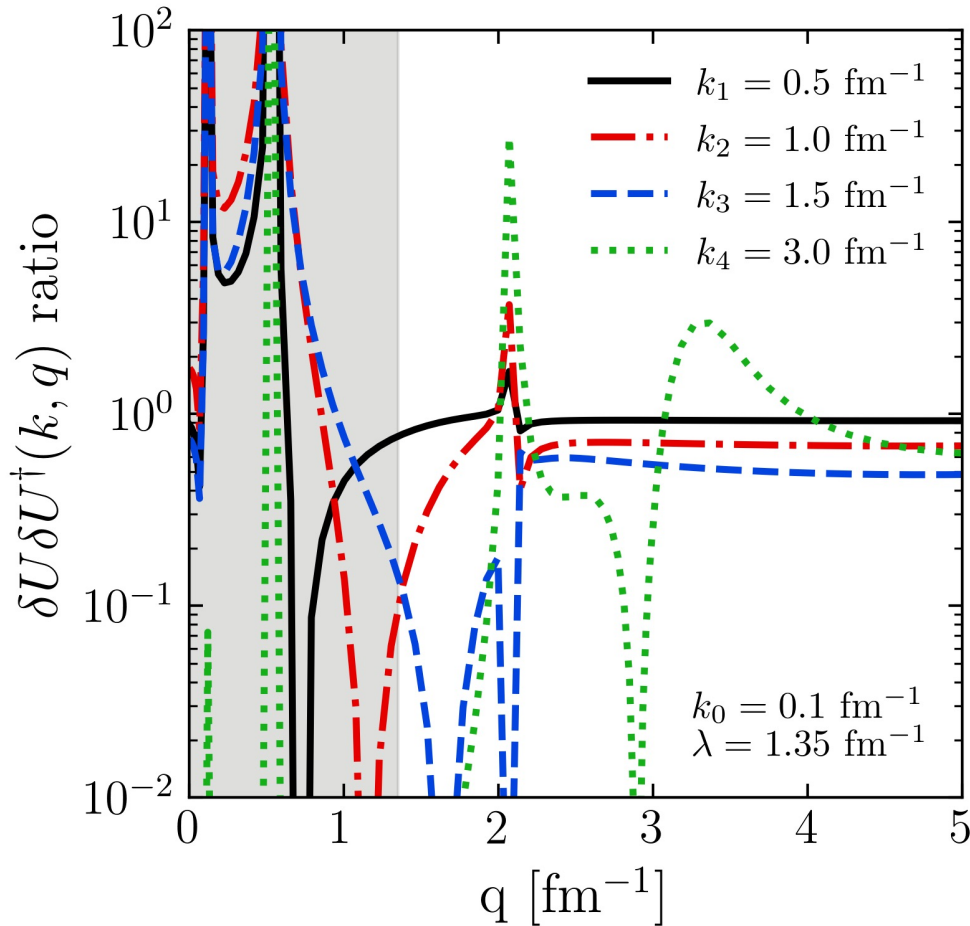


Fig. 19: Ratio of $\delta U \delta U^\dagger(k, q)$ for fixed k and λ .

- Consider an operator dominated by high momentum q where $k < \lambda$ and $q \gg \lambda$
- Expand the eigenstates ψ_α^∞ of the initial NN Hamiltonian in terms of the SRG-evolved states ψ_α^λ

$$\psi_\alpha^\infty(q) \approx \gamma^\lambda(q) \int_0^\lambda d\tilde{p} Z(\lambda) \psi_\alpha^\lambda(p) + \eta^\lambda(q) \int_0^\lambda d\tilde{p} p^2 Z(\lambda) \psi_\alpha^\lambda(p) + \dots$$

- Substitute leading-order term of operator product expansion (OPE) in spectral representation of SRG transformation

$$\begin{aligned} U_\lambda(k, q) &= \sum_{\alpha}^{\infty} \langle k | \psi_\alpha^\lambda \rangle \langle \psi_\alpha^\infty | q \rangle \\ &\approx \left[\sum_{\alpha}^{|E_\alpha| \ll |E_{QHQ}|} \langle k | \psi_\alpha^\lambda \rangle \int_0^\lambda d\tilde{p} Z(\lambda) \psi_\alpha^{\lambda\dagger}(p) \right] \gamma^\lambda(q) \\ &\equiv K_\lambda(k) Q_\lambda(q) \end{aligned}$$